

Journal of Geophysical Research: Oceans**RESEARCH ARTICLE**

10.1002/2014JC010519

Key Points:

- Isoprene and volatile organic iodine were measured in ocean surface water
- High concentrations occur in highly productive waters
- CH_3I sea-to-air flux was dominant in basin areas; CH_2ClI in shelf-slope areas

Supporting Information:

- Supporting Information S1
- Data Set S1

Correspondence to:

A. Ooki,
ooki@fish.hokudai.ac.jp

Citation:

Ooki, A., D. Nomura, S. Nishino, T. Kikuchi, and Y. Yokouchi (2015), A global-scale map of isoprene and volatile organic iodine in surface seawater of the Arctic, Northwest Pacific, Indian, and Southern Oceans, *J. Geophys. Res. Oceans*, 120, 4108–4128, doi:10.1002/2014JC010519.

Received 1 NOV 2014

Accepted 13 MAY 2015

Accepted article online 15 MAY 2015

Published online 7 JUN 2015

A global-scale map of isoprene and volatile organic iodine in surface seawater of the Arctic, Northwest Pacific, Indian, and Southern Oceans**Atsushi Ooki¹, Daiki Nomura², Shigeto Nishino³, Takashi Kikuchi³, and Yoko Yokouchi⁴**

¹Faculty of Fisheries Sciences, Hokkaido University, Hakodate, Japan, ²Institute of Low Temperature Science, Hokkaido University, Sapporo, Japan, ³Institute of Arctic Climate and Environment Research, Japan Agency for Marine-Earth Science and Technology, Yokosuka, Japan, ⁴National Institute for Environmental Studies, Tsukuba, Japan

Abstract Isoprene (C_5H_8) and three volatile organic iodine compounds (VOIs: CH_3I , $\text{C}_2\text{H}_5\text{I}$, and CH_2ClI) in surface seawater were measured in the western Arctic, Northwest Pacific, Indian, and Southern Oceans during the period 2008–2012. These compounds are believed to play an important role in the marine atmospheric chemistry after their emission. The measurements were performed with high time-resolution (1–6 h intervals) using an online equilibrator gas chromatography mass spectrometer. C_5H_8 was most abundant in high-productivity transitional waters and eutrophic tropical waters. The chlorophyll- a normalized production rates of C_5H_8 were high in the warm subtropical and tropical waters, suggesting the existence of a high emitter of C_5H_8 in the biological community of the warm waters. High concentrations of the three VOIs in highly productive transitional water were attributed to biological productions. For CH_3I , the highest concentrations were widely distributed in the basin area of the oligotrophic subtropical NW Pacific, probably due to photochemical production and/or high emission rates from phytoplankton. In contrast, the lowest concentrations of $\text{C}_2\text{H}_5\text{I}$ in subtropical waters were attributed to photochemical removal. Enhancement of CH_2ClI concentrations in the shelf-slope areas of the Chukchi Sea and the transitional waters of the NW Pacific in winter suggested that vertical mixing with subsurface waters by regional upwelling or winter cooling acts to increase the CH_2ClI concentrations in surface layer. Sea-air flux calculations revealed that the fluxes of CH_2ClI were the highest among the three VOIs in shelf-slope areas; the CH_3I flux was highest in basin areas.

1. Introduction

Marine-derived volatile organic compounds (VOCs) are thought to transfer some elements (carbon, sulfur, nitrogen, and halogens) from the sea surface to the atmosphere, where they play crucial roles in atmospheric chemistry if sufficient VOC productions occur to drive a net efflux from the ocean. VOCs provide a sink for OH radicals and are involved in the formation and destruction of ozone (O_3) and the formation of aerosols that serve as cloud condensation nuclei [e.g., Carpenter *et al.*, 2012]. Isoprene (C_5H_8) is the most largely emitted biogenic VOC in the atmosphere. The global C_5H_8 flux accounts for 44% of the total VOC flux (1150 Tg yr^{-1}) [Guenther *et al.*, 1995]. Although terrestrial vegetation accounts for the largest emissions of C_5H_8 , marine-derived C_5H_8 can also influence the oxidation capacity of remote marine air because the lifetime of C_5H_8 in marine air (several hours) is much less than the transport time (several days) from terrestrial sources to remote regions of the ocean [Broadgate *et al.*, 1997; Palmer and Shaw, 2005].

Volatile organic halogen compounds (halocarbons) such as monohalomethane, dihalomethane, and trihalomethane are known to provide halogen atoms to the atmosphere, resulting in catalytic ozone destruction in the troposphere and stratosphere [World Meteorological Organization (WMO), 2010]. In the case of iodine, the IO radical, which is produced in the atmosphere by photolysis of volatile organic iodine compounds (VOIs) such as methyl iodide (CH_3I), diiodomethane (CH_2I_2), and (chloroiodomethane) CH_2ClI , has the potential to deplete ozone in boundary layer air on a wide scale [e.g., Carpenter *et al.*, 1999]. Methyl iodide is the most abundant VOI species in the air [Yokouchi *et al.*, 2011] because of its long lifetime ($\tau = \sim 7$ days) compared with other very short-lived VOIs with lifetimes of just several minutes to hours [Roehl *et al.*, 1997; Mössinger *et al.*, 1998; WMO, 2010]. Long-term atmospheric CH_3I monitoring results indicate that the pattern

of interannual variations correlates well with the Pacific Decadal Oscillation (PDO), suggesting the possibility that CH_3I emissions are affected by global-scale, decadal anomalies related to sea surface temperature (SST). The oceanic emissions of CH_3I may, therefore, be sensitive to future climate change [Yokouchi *et al.*, 2012].

Recently, an extensive global compilation of CH_3I concentrations in ocean surface waters and the atmosphere has enabled global climatological mapping and an estimate of the global oceanic flux of CH_3I [Ziska *et al.*, 2013]. However, there are still areas in the Indian Ocean, Bering Sea, and western Arctic Ocean where no CH_3I measurements have been made. We will compensate the blank area (Indian, NW Pacific, and western Arctic Oceans) of CH_3I measurement.

For many years, CH_3I has been the principal focus of studies on the flux of iodine released from the sea surface, however, recent studies implied that the total flux of very short-lived VOIs, such as CH_2I_2 and CH_2ClI with atmospheric lifetimes of several minutes to hours, is comparable to the flux of CH_3I [Moore and Tokarczyk, 1992; Schall and Heumann, 1993; Carpenter *et al.*, 2000; Chuck *et al.*, 2005; Jones *et al.*, 2010; Yokouchi *et al.*, 2011]. Despite growing recognition of the necessity to consider the horizontal distributions of very short-lived VOIs as well as CH_3I , results for the surface monitoring of those compounds are very few.

One of the final goals of the oceanic VOC study is to estimate the temporal-spatial distribution of VOC flux to the atmosphere on a global scale. The global VOC emission models have been developed for C_5H_8 , bromoform (CHBr_3), CH_3I , and dimethyl sulfide (CH_3SCH_3), of which observational data have been previously compiled to some extent, and validated with results from several observational data [e.g., Simó and Dachs, 2002; Quack and Wallace, 2003; Arnold *et al.*, 2009; Ziska *et al.*, 2013]. Marine biogenic VOCs are thought to be directly emitted from marine biota and probably produced via abiotic reactions of organic matter in seawater [e.g., Happell and Wallace, 1996; Fuse *et al.*, 2003; Hayase *et al.*, 2012]. Both production processes result from the marine primary production; thus, the VOC distributions are expected to be linked to the distributions of photosynthetic pigments in seawater, such as chlorophyll-*a*. Recent model studies have developed to estimate global C_5H_8 emissions from the analysis of phytoplankton functional-type mapping by ocean color satellite images combined with the chlorophyll-*a* normalized phytoplankton-specific C_5H_8 production rates in incubation experiments [Arnold *et al.*, 2009]. On the other hand, the paucity of relevant observations has so far precluded further validation of global oceanic VOC emissions.

What is important in the analysis of observational data for model validation is to obtain a simple global feature of VOC distribution associated with geographical features and oceanic parameters, and thereby, the model parameters can be tuned to represent the feature of VOC distribution for model development. It is also important to obtain net production rates for VOCs assuming a steady state of VOCs in seawater from observational study to compare with the chlorophyll-*a* normalized production rates for specific plankton species measured by incubation experiments. If there is an inconsistency between the net production rates from observational study and the incubation experiments results, it makes us recognize the existence of productions and/or loss of VOCs in seawater which is being overlooked.

In this study, we conducted shipboard measurements to find the concentrations of C_5H_8 and three VOIs (CH_3I , ethyl iodide ($\text{C}_2\text{H}_5\text{I}$), and CH_2ClI) from the Arctic to the Southern Ocean. These data were used to map the horizontal distributions of the concentrations of these compounds in surface mixed layer water, and obtain global features of their distributions and their average fluxes over the atmosphere. Our mapping data (C_5H_8 , CH_3I , $\text{C}_2\text{H}_5\text{I}$, and CH_2ClI) is published as a supplement data of this paper.

We discussed the determining factors in the concentration variability of the compounds among five water types (polar, subpolar, transitional, subtropical, and tropical waters) and three ocean areas (shelf, slope, and basin). Isoprene concentration was parameterized by multiple-regression analysis using chlorophyll-*a* concentration and SST, and the production rates of C_5H_8 and CH_3I were obtained to discuss the characteristics of production processes.

2. Methods

2.1. Ship Observations

VOC measurements were taken in the Southern Ocean, the North and South Indian Oceans, the Northwest (NW) Pacific Ocean, the Bering Sea, and the Pacific sector of the western Arctic Ocean, which includes the

Table 1. Cruise and Sampling Information

Cruise Name	Ship Name	Cruise Period	Sampling Area	Surface Seawater ^a	Air ^b	Chlorophyll-a ^c
HK08-1	Hokko-maru	Jan 2008	NW Pacific	EQ		Underway
KH-08-2	Hakuho-maru	Jul–Sep 2008	NW Pacific	EQ	Online	Underway
KT-09-5	Tansei-maru	Apr–May 2009	NW Pacific	EQ	Online	Underway
KH-09-5	Hakuho-maru	Nov 2009 to Jan 2010	NW Pacific (coastal) Indian Ocean Southern Ocean	EQ	Online	CTD-stations
KH-10-1	Hakuho-maru	May 2010	NW Pacific	EQ		CTD-stations
MR12-E03	Mirai	Sep–Oct 2012	NW Pacific Bering Sea Arctic Ocean	EQ	Canister	Underway Daily
SIPEX-2	Aurora Australis	Sep–Nov 2012	Southern Ocean	P&T		

^aEQ: online equilibrator with GC/MS system for surface mixed layer water measurement. P&T: purge and trap with GC/MS system for discrete seawater sample measurement. The measurement was performed about 2 months later.

^bOnline: online GC/MS system for air measurement. Canister: air measurement by canister sampling. The measurement was done onboard within 2 h after air sampling.

^cUnderway: underway measurement by fluorescence sensor calibrated using the Welschmeyer method. CTD-station: discrete surface mixed layer water samples were collected at CTD observation stations. Daily: discrete surface mixed layer water samples were collected daily. Chlorophyll-a concentration of the discrete samples were measured using the Welschmeyer method.

Arctic Ocean basin and the Chukchi Sea, from 2008 to 2012 aboard the R/V *Hokko-maru* (cruise name HK08-1), R/V *Hakuho-maru* (KH-08-2, KH-09-5, and KH-10-1), R/V *Tansei-maru* (KT-09-5), R/V *Mirai* (MR12-E03), and R/V *Aurora Australis* (SIPEX-2). The cruise and sampling information are listed in Table 1.

2.2. VOC Measurements

Surface mixed layer water was pumped from an intake at the bottom of the ship (~5 m depth) to a silicone membrane tube equilibrator at a flow rate of 15 L min⁻¹ on all cruises except for the SIPEX2-cruise. Details of VOC measurements are described elsewhere [Ooki and Yokouchi, 2008; Ooki et al., 2010]. Briefly, the equilibrator consists of six silicone tubes (length, 10 m; o.d., 2.0 mm; i.d., 1.5 mm) housed in a polyvinyl chloride (PVC) pipe. Pure air was continuously supplied to the silicone tubes at a flow rate of 25 mL min⁻¹, regulating the inner pressure to +0.14 MPa. The gas-phase sample of VOCs at equilibrium with the seawater could be obtained from the outlet of the silicone tube. The collection efficiencies (equilibration level) for C₅H₈ and VOIs were well established by the equilibration level test according to the method by Ooki and Yokouchi [2008]. From the sampling line artifact test performed by changing the equilibrator between a brand-new and a well-used one [Ooki and Yokouchi, 2008; Ooki et al., 2010], significant contaminations or losses of C₅H₈ and VOIs were not confirmed. We conducted routine cleaning (each leg or more frequently) to remove particulate organic matter in the equilibrator with compressed air bubbles introduced into the seawater stream according to the cleaning method [Ooki and Yokouchi, 2008].

The dry air mole fraction of C₅H₈ and the three VOIs in the surface mixed layer water (χ_{water}) in parts per trillion (ppt) were measured onboard with a preconcentration gas chromatograph-mass spectrometer (GC-MS) analytical system at intervals of 1–6 h. The gas-phase sample (750 mL of equilibrated air or outside air as described below) was collected in a trap containing Carboxene 1000 and Carbopak B cooled to –50°C in a small freezer. Concentrated VOCs in this first trap were thermally (200°C) desorbed and transferred to a second trap, which contained Tenax TA and Carboxene 1000 cooled to –50°C. Then the second trap was heated to 200°C, and the desorbed components were transferred to a capillary column (Porabond Q, 0.32 mm, 50 m) for GC-MS analytical system (Agilent 5973, 6890). On the SIPEX2-cruise, surface mixed layer water samples were collected in dark glass bottles (32 mL). For arresting microbial activity, 50 µL of 3.5 (wt %) mercuric chloride (HgCl₂) solution, which had been previously bubbled with high-purity nitrogen (N₂) for 30 min at 90–100°C to remove possible contaminating gases, was added to each bottle. About 2 months later, dissolved VOC concentrations in each seawater sample from SIPEX2 were measured by purge-and-trap (P&T) combined with GC-MS [Ooki and Yokouchi, 2011a]. We investigated the possibility of contamination and the loss of isoprene and three VOIs in the seawater bottle during sample storage (1–6 months). Because the dissolved CH₃I and C₂H₅I concentrations in the sample bottles decreased at a rate of about 10% per month during storage, we believe the CH₃I and C₂H₅I concentrations for the SIPEX2-cruise in the Southern Ocean are underestimates of the initial concentrations by approximately 10–20%. A significant

loss of CH_2ClI was not apparent during 2 months of storage. The concentrations of C_5H_8 in the discrete seawater samples were not quantified because of a loss problem.

The partial pressures of C_5H_8 and three VOIs measured using the equilibrator system were compared with the respective molar concentrations measured using the P&T system to determine their Henry's law constants onboard during the KH-09-5 cruise [Ooki and Yokouchi, 2011b]. Good agreement between the Henry's law constants obtained from our observation and previously reported values ensured validity of our analytical system.

Outside air was drawn from the uppermost deck of the ship on the KH-08-2, KH-09-5, and KT-09-5 cruises. The air sample (750 mL) was introduced to the preconcentration GC-MS system, which was used for surface mixed layer water analysis onboard, at 6–12 h intervals. During the R/V *Mirai* cruise (MR12-E02), outside air was collected in a preevacuated, stainless steel canister (6 L, SilicoCan, Restek Co., Ltd.) on the uppermost deck of the ship approximately once every 2 days. The air sample in the canister was analyzed onboard by the same GC-MS system within 2 h of sampling.

The same procedures were used to analyze gravimetrically prepared standard gases (Taiyo Nissan, Inc., Tokyo) containing C_5H_8 , CH_3I , and $\text{C}_2\text{H}_5\text{I}$ at concentrations of 100 ppt to 10 parts per billion (ppb). The mixed standard gases measurements were carried out once or twice a day. Calibration of the analytical system for CH_2ClI , which was not included in the standard gas, was performed using a methanol-based liquid standard containing CH_2ClI as well as CH_3I , $\text{C}_2\text{H}_5\text{I}$, and C_2Cl_4 . The methanol-based standard (0.5 μL) containing 14 pmol CH_2ClI , 16 pmol CH_3I , 13 pmol $\text{C}_2\text{H}_5\text{I}$, and 10 pmol C_2Cl_4 was analyzed with the same GC-MS system at the beginning and end of each trip. We employed the relative ratios of the CH_2ClI response to the C_2Cl_4 response in the methanol-based standard and samples.

The detection limits (signal/noise = 3) were 0.2 ppt for the three VOIs and 1 ppt for C_5H_8 . The analytical precisions of the $p\text{VOC}$ values were within 1% for all of the species based on replicate analyses of the standard gas.

While CH_2I_2 should be a major component of the VOI emission from the ocean, we could not detect the concentrations of CH_2I_2 in gas-phase sample equilibrated with respect to the surface mixed layer water concentrations by the silicone membrane equilibrator—GC/MS system because of its high solubility in seawater and low concentrations in the surface of open ocean water. Since we could not check the sampling line artifact of CH_2I_2 using the online equilibrator system during the cruise, CH_2I_2 data were not reported in the present study.

2.3. Chlorophyll- α in Surface Mixed Layer Water

Chlorophyll- α (Chl- α) concentrations in surface mixed layer water were continuously monitored with a fluorescence sensor using the surface mixed layer water collected from the bottom of the ship during cruises of KH-08-1, KH-08-2, and KT-09-5. The continuous fluorescence data were calibrated with Chl- α concentrations measured using the fluorometric Welshmeyer method [Welshmeyer, 1994] daily or more frequently. The Chl- α monitoring results for KH-08-2 were previously reported by Ooki *et al.* [2010]. Discrete seawater samples were collected from 5 m (or 10 m) depth using a conductivity-temperature-depth (CTD) rosette water sampling system (KH-09-5 and KH-10-1) from an underway surface mixed layer water (MR-12-E03). The Chl- α concentrations in discrete seawater samples were measured by the Welshmeyer method.

2.4. Partial Pressure and Sea-Air Flux Calculations

The partial pressure $p\text{VOC}$ of a VOC in picoatmospheres (patm) can be calculated from the dry air mole fraction (χ_{VOC}) in ppt using the following equation [Richter, 2003], which assumes ideal gas behavior:

$$p\text{VOC} = (p - p\text{H}_2\text{O})/p \times \chi_{\text{VOC}}, \quad (1)$$

where p is the total pressure (in equilibrator or air) and $p\text{H}_2\text{O}$ is the partial pressure of water vapor.

The concentrations of VOCs (C_{VOC} ; pmol L^{-1}) in seawater were calculated as follows:

$$C_{\text{VOC}} = p\text{VOC}_{\text{water}} \cdot H_{\text{VOC}}, \quad (2)$$

where $p\text{VOC}_{\text{water}}$ is the partial pressure of VOC (patm) in seawater, and H_{VOC} is the temperature-dependent Henry's law constant ($\text{mol L}^{-1} \text{ atm}^{-1}$) obtained from Moore *et al.* [1995] for CH_2ClI and CH_3I , and Ooki and Yokouchi [2011b] for $\text{C}_2\text{H}_5\text{I}$ and C_5H_8 .

Sea-air fluxes of VOCs (F_{VOC} ; nmol m $^{-2}$ d $^{-1}$) were calculated as follows:

$$F_{VOC} = K(pVOC_{water} - pVOC_{air})H_{VOC}, \quad (3)$$

where K is the gas transfer velocity (cm s $^{-1}$), which depends on wind speed; $pVOC_{water}$ and $pVOC_{air}$ are the partial pressures of the VOC in water and air, respectively; and H_{VOC} is the Henry's law constant for the VOC. The gas transfer velocity can be calculated from the *Wanninkhof* [1992] formulation as follows:

$$K = 0.31 \times u^2 (Sc/660)^{-0.5}, \quad (4)$$

where u is the wind speed and Sc is the Schmidt number.

The Schmidt number for VOIs was estimated assuming that the ratio of the diffusivities of methyl bromide (CH₃Br) and VOIs in seawater is inversely proportional to ratio of their molar volumes to the power 0.6 [Wilke and Chang, 1955]. Wilke and Chang estimated an error of 10% using this method. This approach is based on Moore and Groszko [1999], Richter [2003], and Varner *et al.* [2008]. The only methyl halide diffusivity measured is that for methyl bromide (CH₃Br) [DeBruyn and Saltzman, 1997]. They reported $Sc(CH_3Br)$ as function of temperature (T;°C) as follows:

$$Sc(CH_3Br) = 2004 - 93.5 \times T + 1.39 \times T^2. \quad (5)$$

Schmidt number of VOI can be calculated from that of CH₃Br using the molar volume ratio (V_{VOI}/V_{CH_3Br}), as follows:

$$Sc(VOI) = (V_{VOI}/V_{CH_3Br})^{0.6} \times (2004 - 93.5 \times T + 1.39 \times T^2). \quad (6)$$

The molar volumes (V_{VOC}) have been estimated with additive method of Le Bas as cited in physical chemical properties hand book [e.g., Ohe, 2002] to be 52.9 cm 3 mol $^{-1}$ for CH₃Br (C:14.8, H₃:3.7 × 3, Br:27), 62.9 cm 3 mol $^{-1}$ for CH₃I (C:14.8, H₃:3.7 × 3, I:37), 83.8 cm 3 mol $^{-1}$ for CH₂Cl₂ (C:14.8, H₂:3.7 × 2, Cl:24.6, I:37), and 85.1 cm 3 mol $^{-1}$ for C₂H₅I (C₂:14.8 × 2, H₅:3.7 × 5, I:37).

Schmidt number of C₅H₈ ($Sc = \nu/D$) is given from kinetic viscosity of water (ν) and diffusivity of C₅H₈ (D_{C5H8}). We applied the classic Wilke and Chang [1955] equation to the D_{C5H8} calculation, as follows:

$$D_{C5H8} = 7.4 \times 10^{-8} (2.6 \times M)^{0.5} T / (\eta V_a^{0.6}), \quad (7)$$

where M is molar mass of water; T is temperature (K); η is the viscosity of seawater (as cited in Sharqawy *et al.* [2010]); and V_a is the molar volume of C₅H₈ (103.6).

Positive values of the flux indicate a sea-to-air efflux. The $pVOC_{air}$ data measured onboard were used for the flux calculations. Because many $pC_2H_5I_{air}$ and pCH_2Cl_{air} samples were below the detection limit (0.2 patm), fluxes of C₂H₅I and CH₂Cl₂ were calculated using fixed partial pressures of 0 or 0.2 patm for $pC_2H_5I_{air}$ and pCH_2Cl_{air} when the data were below the detection limit.

2.5. Production Rate Calculation

Net production rates, $P(VOC)$, of C₅H₈ and CH₃I in the surface mixed layer were calculated using the mixed layer depth and abiotic loss rates of the compounds, assuming a steady state of the compounds in the surface mixed layer. Note that the production rates of both compounds are the net biological productions and losses. The main process that causes the abiotic loss of C₅H₈ from surface mixed layer water is sea-to-air efflux [Palmer and Shaw, 2005], and the main processes that cause loss of CH₃I are sea-to-air efflux and nucleophilic substitution by chloride [Elliott and Rowland, 1993]. Transport of VOCs from the surface mixed layer to the subsurface layer by diffusive mixing was ignored. $P(C_5H_8)$ and $P(CH_3I)$ values in pmol L $^{-1}$ d $^{-1}$ unit were calculated as follows:

$$P(C_5H_8) = F(C_5H_8) / MLD, \quad (8)$$

$$P(CH_3I) = F(CH_3I) / MLD + Cl\text{-loss}, \quad (9)$$

where $F(VOC)$ is the VOC sea-air flux; MLD is the mixed layer depth, which is the depth where the potential density increases by 0.125 kg m $^{-3}$ compared with the reference depth of 5 m (or 10 m); and $Cl\text{-loss}$ is the nucleophilic substitution loss rate of CH₃I calculated from Jones and Carpenter [2007]. The chlorophyll-a

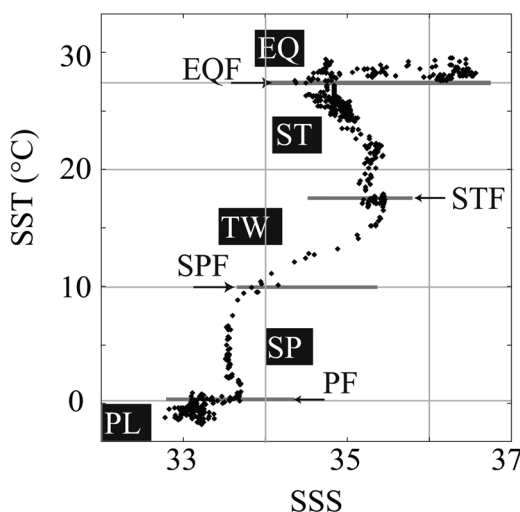


Figure 1. T-S diagram of surface mixed layer water in the Indian Ocean during the KH-09-5 cruise. Water mass types and ocean fronts are denoted by EQ (equatorial tropical water), EQF (equatorial front), ST (subtropical water), STF (subtropical front), TW (transitional water between the ST and SP), SPF (subpolar front), SP (subpolar), PF (polar front), and PL (polar water).

Pacific, Indian, and Southern Oceans. The frontal structure of the NW Pacific is characterized by the subpolar (subarctic) front at 44°N and the Kuroshio extension front at 32°N [Yasuda, 2003; Ooki *et al.*, 2010]. The Chukchi Sea water in the western Arctic Ocean can be regarded as polar water with low salinity (<31); we assumed that the Bering Sea water moved to the Arctic Ocean through the Bering Strait. The latitude bands of subtropical, transitional, subpolar, and polar waters from the NW Pacific to the Arctic Ocean lied between 12°N and 32°N, 32°N and 44°N, 44°N and 65°N, and 65°N and 76°N, respectively.

We assumed that the water masses of the tropical-subtropical Indian Ocean possess salinities greater than 35.1 due to the highly saline water derived from the Arabian Sea and Persian Gulf [Kumar and Prasad, 1999], and the tropical water in the Indian Ocean possess a SST greater than 27.5°C bounded by latitudes of 10°N and 12°N. The latter is the southern boundary of the Intertropical Convergence Zone (ITCZ). The frontal structures of the South Indian and Southern Oceans are bounded by the Agulhas return current in the South Indian Ocean and the Antarctic Circumpolar Current in the Southern Ocean. The values of SST and sea surface salinity (SSS) in transitional waters were taken to be in the range of 10.6–17°C and 34.05–35.35, respectively [Anilkumar *et al.*, 2005]. The Antarctic polar water was taken as low-salinity, cold water (SSS < 33.5, SST < 0°C), which gets affected by meltwater in the area of seasonal sea ice. The fronts in the Indian and Southern Oceans can be noticed in the T-S diagram from the KH-09-5 cruise (Figure 1). In the Indian and Southern Oceans, the latitude bands of tropical, subtropical, transitional, subpolar, and polar waters were found to be in the range of 10°N–12°S, 12°S–37°S, 37°S–44°S, 44°S–59°S, and 59°S–65°S, respectively.

3. Results and Discussion

The partial pressures of VOCs ($\text{VOC} = \text{C}_5\text{H}_8, \text{CH}_3\text{I}, \text{C}_2\text{H}_5\text{I}$, and CH_2ClI) were measured for the surface mixed layer water and air samples on each cruise; a total of 1285 surface mixed layer water samples (numbers in basin, slope, and shelf areas = 972, 196, and 114, respectively) and 233 air samples were collected.

The spatial distributions of the VOC concentrations (pmol L^{-1}) in surface mixed layer water, calculated using equation (2), are shown in (a) of Figures 2, 5–7. The enlarged plots of the western NW Pacific and the Bering Sea-Arctic Ocean regions are shown in (b) of Figures 2, 5–7 and (c) of Figures 2, 5–7, respectively. The concentrations of CH_3I in the NW Pacific on the KH-08-2 cruise and $\text{C}_2\text{H}_5\text{I}$ in the Indian and Southern Oceans on the KH-09-5 cruise were previously reported by Ooki *et al.* [2010] and Ooki and Yokouchi [2011b], respectively. New data are reported here together with these previously reported data.

normalized production rate ($P_{\text{Chl-a}}$) in $(\text{VOC})\mu\text{mol} (\text{Chl-a})\text{g}^{-1} \text{d}^{-1}$ unit was calculated as follows:

$$P_{\text{Chl-a}} = P(\text{VOC}) / \text{ave-Chl-a}, \quad (10)$$

where ave-Chl-a is the average concentration of Chl-a ($\mu\text{g L}^{-1}$) in the mixed layer. Seawater samples for Chl-a measurements were vertically collected by CTD-rosette sampler at CTD observation stations.

2.6. Water Types

To characterize the spatial distributions of VOCs in surface mixed layer water, the sampling area and the water mass were grouped into three areas and five water mass types. The sampling area was categorized divided into shelf areas with bottom depths of <200 m, slope areas with bottom depths of 200–2000 m, and basin areas with bottom depths of >2000 m. The water masses were classified as polar water, subpolar water, transitional water (i.e., a mixture of subpolar and subtropical water), subtropical water, and tropical water based on the frontal structures of the NW

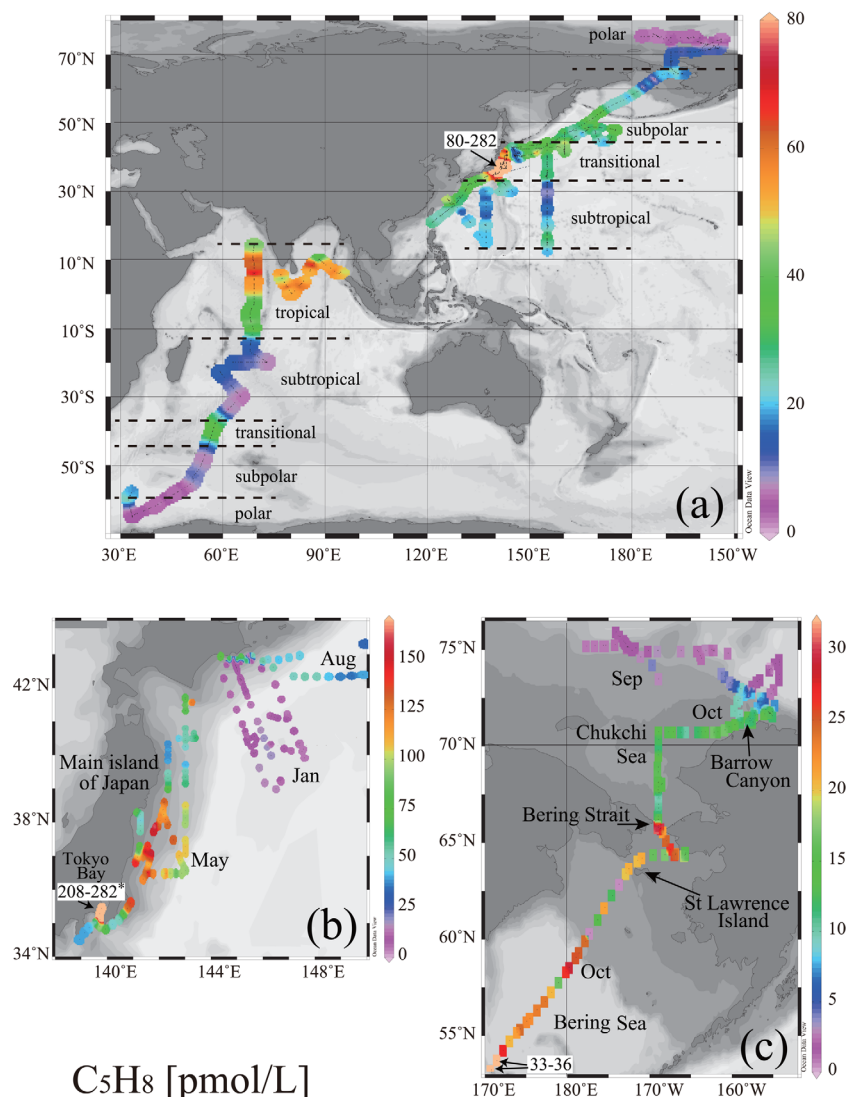


Figure 2. (a) Global-scale map of the horizontal distribution of C_5H_8 concentrations in surface mixed layer water and (b) enlarged maps of C_5H_8 concentrations in the western NW Pacific around Japan and (c) in the Bering Sea and Arctic Ocean. Numbers denoted in the figure with arrows show the concentrations over the color bar range, which were painted in cream-white color symbol.

The average concentrations of VOC in each water type in the basin, slope, and shelf areas are summarized in Table 2. The partial pressures of C_2H_5I and CH_2ClI in seawater for several samples were noticed to be below the detection limit (0.2 patm). The average concentrations in pmol L^{-1} were calculated using the fixed $pVOC_{\text{water}}$ values (0 or 0.2 patm) for C_2H_5I and CH_2ClI when the data were below the detection limit. The average values and ranges of Chl- α concentration in surface mixed layer water samples are summarized in Table 2. Correlation analysis results of VOCs concentrations are listed in Table 3.

3.1. Isoprene (C_5H_8)

From the statistical analysis, the average concentrations (min-max) of C_5H_8 in all water types in basin, slope, and shelf areas were calculated to be 27 (1.3–121), 44 (1.5–165), and 30 (2.7–136) pmol L^{-1} , respectively. In the basin areas, the tropical water had the highest average (50 pmol L^{-1}) and the polar water had the lowest average (4.2 pmol L^{-1}).

From the global map of C_5H_8 distribution, high-productivity shelf-slope areas in transitional water were observed to have the highest average values (74 – 96 pmol L^{-1}) among all the water and area types. The highest concentrations of C_5H_8 (75 – 165 pmol L^{-1}) were localized to the transitional waters of shelf and

Table 2. Average (Min, Max) Concentrations of VOC (pmol/L) and Chlorophyll-*a* ($\mu\text{g}/\text{L}$) in Basin (Bottom Depth > 2000 m), Slope (200–2000 m), and Shelf (<200 m) Areas

Water Type	Latitude Bands (Indian, NW Pacific)	SST	C_5H_8	CH_3I	$\text{C}_2\text{H}_5\text{I}$	CH_2ClI	Chlorophyll- <i>a</i>
<i>Polar water (59°S–65°S, 65°N–76°N)</i>							
Basin (n = 96)		−0.6 (−1.8, 3.9)	4.2 (1.3, 16)	1.5 (0.57, 3.8)	0.16–0.17 ^a (DL, 0.44)	0.37–0.76 (DL, 7.4)	0.49 (0.05–0.99)
Slope (n = 85)		0.5 (−1.6, 4.0)	4.4 (1.5, 14)	1.0 (0.62, 1.9)	0.11–0.13 (DL, 0.65)	2.9–3.1 (DL, 14)	0.12 (0.07–0.25)
Shelf (n = 60)		2.9 (0.1, 5.2)	13 (2.7, 31)	1.4 (0.78, 2.1)	0.44 (0.11, 1.0)	5.7 (DL, 12)	0.96 (0.4–1.4)
<i>Subpolar water (44°S–59°S, 44°N–65°N)</i>							
Basin (n = 186)		11 (0.0, 17)	27 (2.2, 60)	3.6 (1.0, 9.1)	0.17 (DL, 0.49)	0.35–0.60 (DL, 4.1)	0.70 (0.28–1.8)
Slope (n = 1)		6	25	2.4	0.17	0.98	
Shelf (n = 20)		3.0 (1.3, 5.6)	19 (12, 26)	2.5 (1.5, 4.1)	1.3 (0.13, 2.7)	2.9 (0.95, 6.1)	0.97 (0.9–1.0)
<i>Transition water (37°S–44°S, 32°N–44°N)</i>							
Basin (n = 339)		16 (0.1, 29)	33 (6.4, 121)	3.7 (1.1, 8.4)	0.20 (0.05, 3.2)	1.3–1.4 (DL, 15)	0.69 (0.08–6.0)
Slope (n = 60)		13 (3.4, 19)	92 (37, 165)	4.0 (1.5, 7.9)	0.49 (0.08, 2.5)	5.1 (0.3, 19)	3.3 (0.16–10.3)
Shelf (n = 27)		16 (3.5, 26)	74 (39, 136)	5.3 (1.4, 12)	0.69 (0.07, 4.0)	12 (1.3, 93)	2.4 (0.4–7.0)
<i>Subtropical water (12°S–37°S, 12°N–32°N)</i>							
Basin (n = 264)		26 (17, 30)	17 (5.4, 34)	4.8 (2.0, 8.3)	0.08 (0.04, 0.17)	0.54–0.55 (DL, 4.6)	0.05 (0.03–0.12)
Slope (n = 50)		25 (22, 27)	33 (20, 50)	2.4 (1.5, 3.4)	0.06 (0.04, 0.15)	3.4 (0.92, 6.0)	
Shelf (n = 7)		24 (23, 25)	42 (34, 49)	2.9 (1.6, 5.0)	0.11 (0.05, 0.24)	2.5 (1.6, 3.7)	
<i>Tropical water (10°N–12°S)</i>							
Basin (n = 87)		28 (27, 30)	50 (29, 75)	3.4 (1.8, 6.6)	0.08 (0.06, 0.12)	2.3 (0.45, 5.8)	0.16 (0.09–0.19)
<i>Total</i>							
Basin (n = 972)		17 (−1.8, 30)	27 (1.3, 121)	3.7 (0.57, 9.1)	0.15 (DL, 3.2)	0.93–1.0 (DL, 15)	
Slope (n = 196)		10 (−1.6, 29)	44 (1.5, 165)	2.3 (0.62, 7.9)	0.23–0.24 (DL, 2.5)	3.7–3.8 (DL, 19)	
Shelf (n = 114)		7.4 (0.1, 26)	30 (2.7, 136)	2.6 (0.78, 12)	0.59 (0.05, 2.7)	6.6 (DL, 93)	

^aDL means below detection limits samples (<0.2 patm). The average was calculated using a fixed range of pVOC_{water} (0–0.2 patm) when the data were below the detection limit (<0.2 patm). The range of average value is attributable to the fixed range of DL sample.

slope areas in the western NW Pacific near Japan in May (Figure 2b; green-to-red symbols and white symbols), where the phytoplankton spring bloom occurred, and Chl-*a* concentrations were markedly high (4.1–10.3 $\mu\text{g}/\text{L}$). The elevated concentrations (208–282 pmol L^{-1} ; denoted with “*” and painted in cream-white color symbol in Figure 2b) in the Tokyo Bay, which is an inner bay, were excluded from the statistical data presented in Table 2. All the data used for the statistical analysis were obtained from the open ocean or a coastal ocean facing the open ocean. The second highest concentrations (50–75 pmol L^{-1}) were widely distributed in the tropical Indian Ocean (Figure 2a; yellow-to-red symbols), where the phytoplankton biomass was relatively higher than that of the oligotrophic subtropical ocean. The Chl-*a* concentrations (~0.16 $\mu\text{g}/\text{L}$) in the tropical Indian Ocean were higher than that of the oligotrophic subtropical ocean (~0.05 $\mu\text{g}/\text{L}$), which is probably due to equatorial upwelling. Moderately high concentrations (30–50 pmol L^{-1} ; green symbols in Figure 2a) were widely distributed from transitional to subpolar waters of the NW Pacific between 35°N and 55°N, whereas in the South Indian Ocean, moderately high concentrations were observed in a narrow latitude band between 35°S and 45°S in transitional waters. These transitional waters

Table 3. Correlation Coefficients (R) for Each VOC Concentration^a

Water Type	C_5H_8	CH_3I	$\text{C}_2\text{H}_5\text{I}$	CH_2ClI	CH_3I	$\text{C}_2\text{H}_5\text{I}$	CH_2ClI
Latitude Bands (Indian, NW Pacific)	CH ₃ I	C ₂ H ₅ I	CH ₂ ClI	C ₂ H ₅ I	CH ₃ I	CH ₂ ClI	C ₂ H ₅ I
<i>Polar water (59°S–65°S, 65°N–76°N)</i>							
Basin (n = 96)	0.53	0.49	0.16	0.21	0.07	0.07	
Slope (n = 85)	0.93	0.84	0.77	0.62	0.40	0.36	
Shelf (n = 60)	0.71	0.63	0.05	0.75	0.04	0.20	
<i>Subpolar water (44°S–59°S, 44°N–65°N)</i>							
Basin (n = 186)	0.71	0.28	0.01	0.49	0.57	0.13	
Slope (n = 1)							
Shelf (n = 20)	0.45	0.37	−0.05	0.60	0.23	0.47	
<i>Transition water (37°S–44°S, 32°N–44°N)</i>							
Basin (n = 339)	0.12	0.57	0.00	0.38	0.30	0.00	
Slope (n = 60)	0.27	0.30	0.10	0.42	0.36	0.03	
Shelf (n = 27)	0.13	0.12	0.01	0.69	0.66	0.13	
<i>Subtropical water (12°S–37°S, 12°N–32°N)</i>							
Basin (n = 264)	0.58	0.33	0.31	0.23	0.10	0.17	
Slope (n = 50)	0.09	0.65	−0.50	0.37	0.45	−0.67	
Shelf (n = 7)	0.38		−0.42		0.31		
<i>Tropical water (10°N–12°S)</i>							
Basin (n = 87)	0.13	0.22	0.61	0.01	0.04	−0.59	

^aHigh correlations (greater than 0.60) are shown in bold.

^bC₂H₅I concentrations for five samples were below the detection limit.

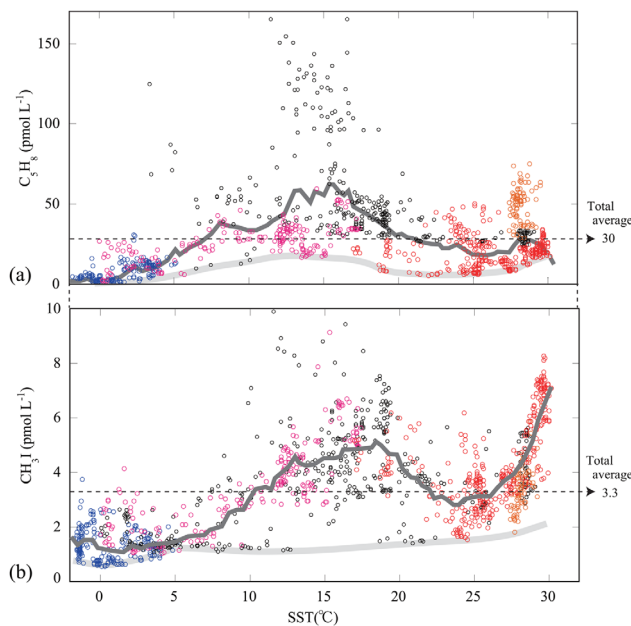


Figure 3. Scatterplots of (a) C_5H_8 versus SST and (b) CH_3I versus SST in basin areas. Bold black lines and gray lines indicate the weighted averages and baselines, respectively. Water types, denoted by colored circles, are polar water (blue), subpolar (purple), transition (black), subtropical (red), and tropical (orange).

low concentrations have been observed in the transitional waters of the western NW Pacific ($6.3\text{--}30\text{ pmol L}^{-1}$) in April during a diatom bloom ($Chl-a = 1\text{--}3\text{ }\mu\text{g L}^{-1}$) [Kurihara *et al.*, 2010], probably during the early phase of the bloom, because in that area phytoplankton spring blooms usually commence in April and terminate in May [Saito *et al.*, 2002]. It is considered that, in high-productivity areas, C_5H_8 accumulates in water columns throughout the bloom period from the early phase of the bloom to the terminal phase. The spatial variability of C_5H_8 concentrations in the high-productivity transitional NW Pacific (Figure 2b) could be caused due to the nonuniformity of the bloom phase as well as differences in the magnitude of the bloom.

In subpolar and polar waters, Tran *et al.* [2013] reported that the lowest concentrations (mean 14.5 pmol L^{-1}) were noticed in the Atlantic sector of the Arctic Ocean, the second lowest concentrations (mean $23.4\text{--}24.8\text{ pmol L}^{-1}$) were noticed in the subpolar Atlantic, and highest concentrations (mean 42.5 pmol L^{-1}) were noticed in the warm, subpolar Atlantic Ocean during June–July. These low concentrations in polar–subpolar waters are consistent with our results. In coastal areas, Baker *et al.* [2000] reported elevated concentrations ($21\text{--}46\text{ pmol L}^{-1}$) in subpolar waters of the Atlantic slope area near Mace Head in May, and Broadgate *et al.* [1997] observed a strong seasonal cycle in subpolar coastal waters of the North Sea, with a maximum concentration of 54 pmol L^{-1} in May.

3.1.1. Relationship Between C_5H_8 Concentration and SST

We examined the relationship between C_5H_8 concentrations and SSTs in basin areas (Figure 3a). We found the maximum C_5H_8 concentration at temperatures between 10 and 20°C , which corresponds to the temperature range associated with phytoplankton blooms in transitional and subpolar waters. We also observed that the maximum C_5H_8 concentration ($>50\text{ pmol L}^{-1}$) in the eutrophic tropical Indian Ocean occurred in areas where the SST was high, i.e., approximately 28°C (orange symbols in Figure 3a). We examined the production rate of C_5H_8 in each water type, and a regression analysis was performed to predict C_5H_8 concentration with relation to the $Chl-a$ concentration and SST (section 3.1.3).

3.1.2. Production Rates

Sea-air flux (F), production rate (P), and $Chl-a$ normalized production rate (P_{Chl}) at CTD-rosette sampling stations were averaged for different water types for each cruise (Table 4). The mean P_{Chl} values were scattered, ranging from 0.4 to $60.5\text{ }\mu\text{mol } (Chl-a)\text{ g}^{-1}\text{ d}^{-1}$. The lowest values ($0.4\text{--}2.8\text{ }\mu\text{mol } (Chl-a)\text{ g}^{-1}\text{ d}^{-1}$) were obtained from cold polar waters (-0.3 to 2.1°C) of the Arctic (September–October) and Southern

have a higher $Chl-a$ concentration (average $0.69\text{ }\mu\text{g L}^{-1}$) than the subtropical and tropical waters. The second lowest concentrations of C_5H_8 ($10\text{--}30\text{ pmol L}^{-1}$; blue-to-light blue symbols in Figure 2a) were widely distributed in the basin areas of the oligotrophic subtropical South Indian and NW Pacific Oceans with the lowest average value of $Chl-a$ ($0.05\text{ }\mu\text{g L}^{-1}$). The lowest concentrations ($<10\text{ pmol L}^{-1}$; purple symbols in Figure 2a) were observed in the basin areas of the Arctic and Southern Oceans, where the average $Chl-a$ concentration was $0.49\text{ }\mu\text{g L}^{-1}$.

Previous studies have reported similar high concentrations in the basin area of the subtropical Florida Strait (maximum 51 pmol L^{-1}) in September [Milne *et al.*, 1995], the eutrophic subtropical N Atlantic water west of the African coast ($40\text{--}160\text{ pmol L}^{-1}$) [Zindler *et al.*, 2014], and the transitional waters of the western NW Pacific (maximum 99 pmol L^{-1}) in May [Matsunaga *et al.*, 2002]. In contrast,

Table 4. Sea-Air Flux and Production Rates of C₅H₈ at CTD Stations

Water Types Ocean ^a /Month (n ^b)	MLD (m)/Chl- <i>a</i> ($\mu\text{g L}^{-1}$)	Temp. (°C)	Wind Speed (m s ⁻¹)	Conc. (pmol L ⁻¹)	Sea-Air Flux (nmol m ⁻² d ⁻¹)	Net Production (pmol L ⁻¹ d ⁻¹)	Chl- <i>a</i> Normalized Production Rate ($\mu\text{mol g}^{-1} \text{d}^{-1}$)
<i>Polar</i>							
Arc/Sep–Oct (26)	16/0.72	2.1	8.4	9.5	23.8	1.6	2.8
S/Dec–Jan (1)	10/0.53	-0.3	8.0	5.6	14.5	1.5	2.7
<i>Subpolar</i>							
NW/Aug (8)	14/0.66	13.9	6.8	30.1	76.4	5.2	8.4
<i>Transitional</i>							
NW/Jan (9)	92/0.53	3.5	6.5	12.4	21.4	0.2	0.4
NW/May (4)	34/4.57	10.9	4.8	114.1	143.8	7.0	1.9
NW/Aug (6)	19/0.19	23.5	5.1	27.9	55.6	2.8	13.7
SI/Dec (1)	26/0.36	17.4	11.3	34.9	232.3	8.9	24.8
<i>Subtropical</i>							
NW/Jun (4)	21/0.08	24.5	6.3	17.5	44.0	2.3	31.4
NW/Sep (4)	35/0.05	28.9	4.6	17.9	29.5	0.9	22.9
SI/Dec (2)	18/0.05	23.4	6.9	6.5	25.9	2.5	60.5
<i>Tropical</i>							
I/Nov–Dec (6)	32/0.18	28.3	4.1	51.9	7.3	2.1	13.6

^aArc: Arctic Ocean, S: Southern Ocean, NW: NW Pacific Ocean, SI: South Indian Ocean, I: North and South Indian Oceans.^bn: number of samples collected at CTD observation stations.

(December) Oceans and cool transitional water (3.5–10.9°C) of the NW Pacific (January and May). These low values are similar to previously reported values (ave. 2.8, 0.07–32.7 $\mu\text{mol} (\text{Chl-}a)\text{g}^{-1} \text{d}^{-1}$) estimated from turnover of C₅H₈ in the surface mixed layer of subpolar-polar waters of the North Atlantic [Tran et al., 2013] and 0.4–1.3 $\mu\text{mol} (\text{Chl-}a)\text{g}^{-1} \text{d}^{-1}$ for diatoms prevailing in the temperate-cold waters measured in phytoplankton incubation experiments [Bonsang et al., 2010], whereas the P_{Chl} values (13.6–60.5 $\mu\text{mol} (\text{Chl-}a)\text{g}^{-1} \text{d}^{-1}$) of warm transitional waters (17.4–23.5°C) during midsummer (August and December) and subtropical-tropical waters (23.4–28.9°C) were 1 order of magnitude higher than the results for cool-cold waters and previous incubation experiments for diatoms. Note that the second highest P_{Chl} value (24.8 $\mu\text{mol} (\text{Chl-}a)\text{g}^{-1} \text{d}^{-1}$) in the South Indian Ocean in December is largely affected by the highest sea-air flux due to the highest average wind speed (11 m s⁻¹). When we regard the second highest rates (24.8 $\mu\text{mol} (\text{Chl-}a)\text{g}^{-1} \text{d}^{-1}$) as an exception, the high production rates (13.6–60.5 $\mu\text{mol} (\text{Chl-}a)\text{g}^{-1} \text{d}^{-1}$) are associated with warmer waters (23.4–28.9°C). The high production rates have been previously reported to be $9.66 \pm 5.78 \mu\text{mol}^{-1} (\text{Chl-}a)\text{g}^{-1} \text{d}^{-1}$ for *Prochlorococcus* [Arnold et al., 2009] and $4.97 \pm 2.87 \mu\text{mol}^{-1} (\text{Chl-}a)\text{g}^{-1} \text{d}^{-1}$ for *Synechococcus* [Bonsang et al., 2010], which are dominant phytoplankton species in the warm tropical-subtropical oceans. We considered that the high production rates found in the warm waters were attributed to the presence of high emitter of C₅H₈ in those waters, such as *Prochlorococcus* and *Synechococcus*, however, there is a large discrepancy between the P_{Chl} values in warm waters from our observations and the previously reported values from incubation experiments.

The production rate of C₅H₈ would depend on the temperature directly linked to the photosynthesis rate. The maximum C₅H₈ production rate by the cyanobacterium *Prochlorococcus* sp. MED4 strain, with a temperature tolerance range of 12.5–28°C, has been observed at 24°C; this is also the temperature that maximizes the photosynthesis rate of this species [Shaw et al., 2003]. The *Prochlorococcus* sp. MED4 strain dominated in the surface layer of midlatitudes (30°N–40°N, 30°S–40°S) in the Atlantic Ocean, and the *Prochlorococcus* sp. MIT9312 strain with a temperature tolerance range between 15 and ~30°C dominated in the lower latitudes (30°N–30°S). Thus, the inconsistency between the high rates of P_{Chl} values in the warm waters obtained from our observations and the low rates of previously reported values from incubation experiments implies the existence of a strong C₅H₈ emitter in warm waters which has not yet been sampled for the incubation experiment.

For temperature dependency of C₅H₈ production by plants other than phytoplankton, the rate of C₅H₈ production by macroalgae is greater by a factor of 4–10 when the incubation temperature is 27.3°C compared to 7.5°C [Broadgate et al., 2004]. The C₅H₈ production by terrestrial higher plants has been studied by many researchers. Sharkey and Yeh [2001] reviewed the C₅H₈ production mechanisms of the terrestrial plants. A number of terrestrial plants emit C₅H₈ in a highly light and temperature-dependent manner that C₅H₈

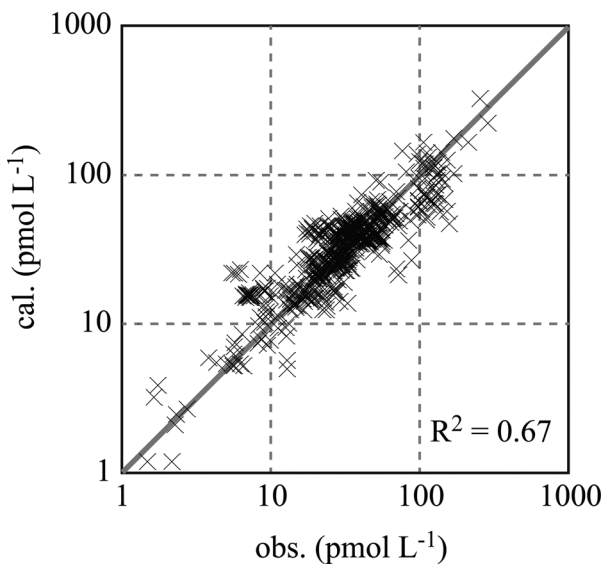


Figure 4. Scatterplot of observed C_5H_8 concentrations versus calculated concentrations. The concentrations were calculated from the regression analysis results.

cyanobacterium *Prochlorococcus* sp. MED4 strain. Further research on the C_5H_8 production processes linked to the biological communities and temperature variance are needed to investigate the C_5H_8 distributions in the ocean and their sea-to-air flux patterns.

3.1.3. Multiple-Regression Analysis

Multiple-regression analysis was carried out to predict C_5H_8 concentrations using the basic oceanic parameters Chl-*a* and SST. We could not obtain an empiric formula to predict C_5H_8 concentrations covering the whole SST range by the regression analysis. When the analytical data were separated into four SST ranges: SST < 3.3°C, 3.3–17, 17–27, and >27°C, we could obtain four empiric formulae to predict C_5H_8 concentrations with the high values for the coefficient of determination ($R^2 = 0.64$ –0.77). A scatterplot of observed versus calculated C_5H_8 concentrations using four formulae is shown in Figure 4. The overall coefficient of determination was $R^2 = 0.67$. A feasible formulae for prediction of C_5H_8 concentrations from Chl-*a* and SST data were obtained (Table 5).

Slope (9.8) for variable [Chl-*a*] in the coldest temperature range (SST < 3.3°C) was smaller than the slopes (14.3–319) in the warmer SST ranges. Similar slope (6.4) for variable [Chl-*a*] has been reported by a single-regression analysis of C_5H_8 concentration in the North Sea and the Southern Ocean [Broadgate et al., 1997]. Recent model studies have developed the global oceanic C_5H_8 flux using the global distribution of phytoplankton functional type and the phytoplankton-specific C_5H_8 productivities [Arnold et al., 2009]. Our regression analysis results would contribute to the validation and development of recent model studies.

3.2. Volatile Organic Iodine Compounds

3.2.1. Methyl Iodide (CH_3I)

The average concentrations (min–max) of CH_3I in all water types in basin, slope, and shelf areas were 3.7 (0.57–9.1), 2.3 (0.62–7.9), and 2.6 (0.78–12) pmol L⁻¹, respectively. From the global map of CH_3I distribution, the highest concentrations of CH_3I (7–11 pmol L⁻¹; shown as red plots in Figure 5a, and light green-red plots in

emission increases with increasing leaf temperature. Terrestrial high plants have been proposed to emit C_5H_8 to the air for temperature regulation, antioxidant (react with ozone and hydroxyl radicals on the leaf), or getting rid of excess energy as by-product of photosynthesis, based on a series of studies.

For marine plants, former two hypotheses (temperature regulation and antioxidant) would be inappropriate in a reason for C_5H_8 emission. While there is no information about the reason for C_5H_8 emission by marine plant, we speculate that marine plants emit C_5H_8 as by-product of photosynthesis. Thus, phytoplankton could be thought to actively produce C_5H_8 at the temperature that maximizes the photosynthesis rate of the species, as the result of incubation experiment by Shaw et al. [2003] for the

Table 5. Regression Analyses for C_5H_8 Concentration (pmol L⁻¹) Using Explanatory Variables Chl-*a* (C; µg L⁻¹) and SST (T; °C)^a

SST Ranges	C_5H_8 (pmol L ⁻¹)
SST < 3.3°C (Chl- <i>a</i> = 0.05–1.44 µg L ⁻¹)	9.80C + 1.49T + 0.649 ($R^2 = 0.71$, p; < 10 ⁻⁴ , 0.005, 0.51)
SST = 3.3–17°C (Chl- <i>a</i> = 0.25–19.8 µg L ⁻¹)	14.3C + 2.27T + 2.83 ($R^2 = 0.64$, p; < 10 ⁻⁹ , < 10 ⁻⁴ , 0.67)
SST = 17–27°C (Chl- <i>a</i> = 0.04–6.49 µg L ⁻¹)	20.9C – 1.92T + 63.1 ($R^2 = 0.77$, p; < 10 ⁻⁹ , < 10 ⁻⁹ , < 10 ⁻⁹)
SST > 27°C (Chl- <i>a</i> = 0.03–0.19 µg L ⁻¹)	319C + 8.55T – 244 ($R^2 = 0.75$, p; < 10 ⁻⁹ , < 10 ⁻⁹ , < 10 ⁻⁹)

^ap = p values; C, T = y intercept.

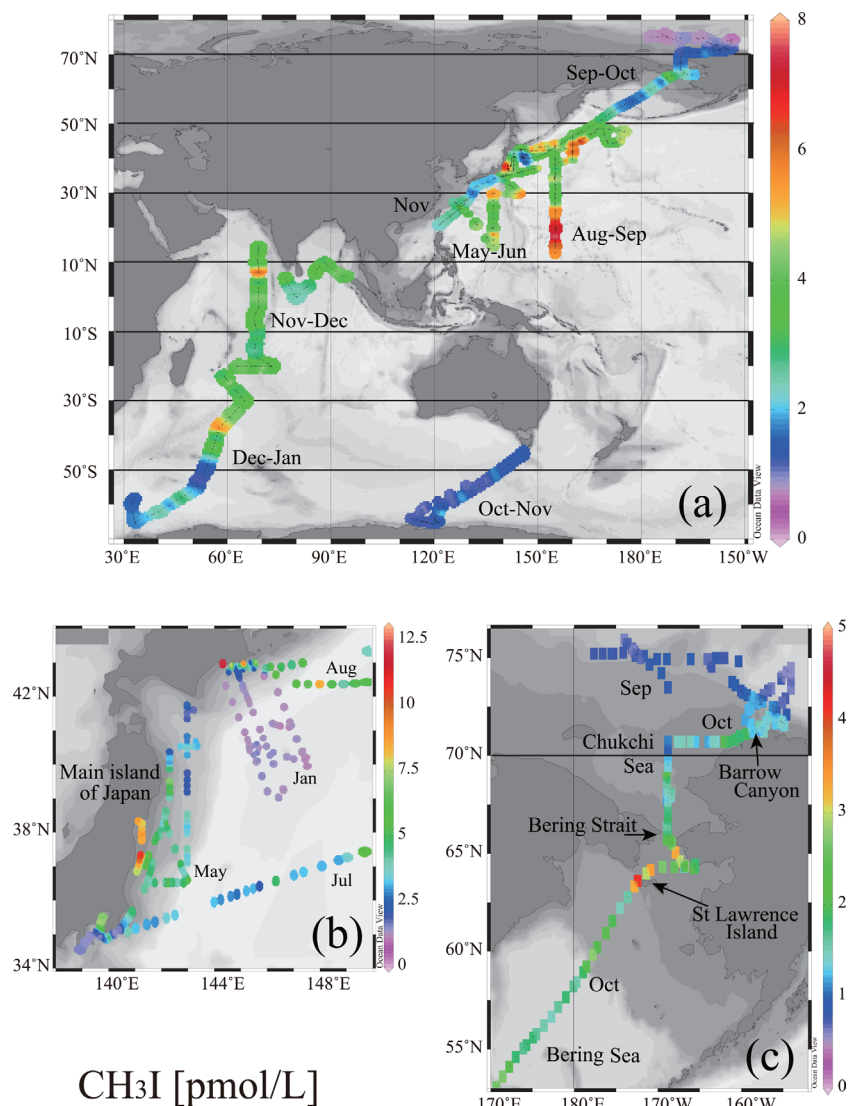


Figure 5. (a) Global-scale map of the horizontal distribution of CH_3I concentrations in surface mixed layer water and (b) enlarged maps of CH_3I concentrations in the western NW Pacific around Japan and (c) in the Bering Sea and Arctic Ocean.

Figure 5b) were localized in shelf-slope areas of the western NW Pacific (Figure 5b) where the $\text{Chl-}\alpha$ concentrations were high ($0.4\text{--}3.8 \mu\text{g L}^{-1}$). High levels of CH_3I occur widely in the basin area of the oligotrophic subtropical NW Pacific (Figure 5a), with the lowest level of $\text{Chl-}\alpha$ ($0.03\text{--}0.06 \mu\text{g L}^{-1}$). The area of high concentration probably extended to the subtropical NW Pacific gyre in summer, because similarly high concentrations of CH_3I (avg. 6.6 pmol L^{-1}) have been observed in the open-ocean part of the oligotrophic subtropical Atlantic Ocean ($26^\circ\text{N}\text{--}36^\circ\text{N}$) [Jones *et al.*, 2010]. The second highest concentrations ($5\text{--}7 \text{ pmol L}^{-1}$; shown as yellow-red plots in Figure 5a, and light blue-green plots in Figure 5b) occurred in highly productive transitional waters of the NW Pacific and South Indian Oceans, and eutrophic tropical water of the Indian Ocean.

The elevated concentrations in high-productivity transitional waters are consistent with previous studies. Chuck *et al.* [2005] reported locally high concentrations of CH_3I in the NE Atlantic (approximately $5\text{--}10 \text{ pmol L}^{-1}$) in the African coastal upwelling system, and in the Southern Ocean between 40°S and 45°S (approximately $5\text{--}19 \text{ pmol L}^{-1}$) in the area of mixing. Moore and Groszko [1999] observed elevated concentrations of CH_3I (up to $7.2\text{--}8.2 \text{ pmol L}^{-1}$) in the subpolar and transitional waters of the North Atlantic. A climatological map of CH_3I concentrations showed high concentrations ($2\text{--}9 \text{ pmol L}^{-1}$) in the subtropical gyres of both the hemispheres and locally high concentrations (up to 9 pmol L^{-1}) in upwelling and coastline regions [Ziska *et al.*, 2013].

Moderate concentrations (3–5 pmol L⁻¹; shown as green plots in Figure 5a, light blue-green plots in Figure 5b, and yellow-red plots in Figure 5c), which are close to the total basin average (3.7 pmol L⁻¹), were widely distributed from tropical-to-subpolar waters. Although the local maxima of CH₃I were often observed near coasts and over the continental shelf within narrow regions, the average for all water types in basin areas (3.7 pmol L⁻¹) was higher than the average values in shelf-slope areas (2.3–2.6 pmol L⁻¹; Table 2).

The CH₃I concentrations dropped sharply at the subpolar front near 44° (for both northern and southern latitudes) toward the subpolar gyre (Figure 5a). The second lowest concentrations (1–3 pmol L⁻¹; shown as blue-light blue plots in Figure 5a, blue plots in Figure 5b, and light blue-yellow in Figure 5c) were widely distributed from subarctic to polar waters. The lowest concentrations (<1 pmol L⁻¹; shown as purple plots in Figure 5a) were widely distributed in the basin area of the Arctic Ocean. These low concentrations are consistent with those reported in previous studies. Chuck *et al.* [2005] observed the lowest concentrations (0.25–2 pmol L⁻¹) in the subpolar South Atlantic and Southern Ocean, and Abrahamsson *et al.* [2004] also reported concentrations of 0.81–1.8 pmol L⁻¹ in the Southern Ocean.

3.2.2. Sources of CH₃I in the Ocean

High correlations ($R = 0.71\text{--}0.93$) between CH₃I and C₅H₈ concentrations in polar-subpolar waters (Table 3) suggest that phytoplankton production of CH₃I is related to biological activity. In high-productivity transitional waters, however, the correlation between CH₃I and C₅H₈ concentrations is poor ($R = 0.12\text{--}0.27$). Nevertheless, the regionally high concentrations of CH₃I in those areas presumably result from biological production of CH₃I by phytoplankton and macroalgae [Manley and Dastoor, 1987; Manley, 1992; Manley and de la Cuesta, 1997]. Phytoplankton production of CH₃I associated with photosynthesis in transitional waters might be more complex than that of polar-subpolar waters because the marine biota in transitional waters (meeting region of warm and cold waters) is thought to be more inhomogeneous than the cold-water biotas. The other high concentrations in oligotrophic subtropical waters may be due to photochemical production of CH₃I [Moore and Zafiriou, 1994; Happell and Wallace, 1996; Yokouchi *et al.*, 2001; Richter and Wallace, 2004; Chuck *et al.*, 2005; Yokouchi *et al.*, 2008] and/or production by cyanobacteria such as *Prochlorococcus* sp., which are one of the most abundant photosynthetic organisms in subtropical waters [Smythe-Wright *et al.*, 2006]. In cold, pelagic waters, where the lowest concentrations of CH₃I were observed, phytoplankton production of CH₃I may be low, even though biological productivity is relatively higher in summer; hence, the rate of production of CH₃I in seawater is probably temperature dependent.

3.2.3. Production Rates of CH₃I

The net production rate of CH₃I was calculated from the sea-air flux and nucleophilic substitution with chloride (Cl-loss). The average values for loss rates and net production rates are summarized in Table 6. The highest air-sea flux (43.8 nmol m⁻² d⁻¹) in the South Indian Ocean in December is largely due to the highest average wind speed (11 m s⁻¹). Cl-loss was the main loss process in subtropical and tropical waters with SST higher than 28°C, accounting for 68–71% of the total loss (air-sea flux and Cl-loss). Cl-loss was a minor in waters with SST = 23–25°C, accounting for 18–35% of the total loss, and in waters with SST less than 17.4°C, it made up 0.4–20% of the total loss. No noticeable differences in net production rates were observed between different types of waters. For the chlorophyll-*a* normalized production rate (P_{Chl}), the values in oligotrophic subtropical waters (15.4–40.4 μmol (Chl-*a*)g⁻¹ d⁻¹) were 1–2 orders of magnitude higher than that in other water types (0.06–5.0 μmol (Chl-*a*)g⁻¹ d⁻¹). Although high rates of P_{Chl}(C₅H₈) production were observed in warm subtropical and tropical waters (Table 4), high rates of P_{Chl}(CH₃I) production were observed only in oligotrophic subtropical water (Table 6). Chuck *et al.* [2005] suggested that CH₃I production is associated with nitrate reductase activity, which could explain the strong negative correlation between CH₃I concentrations and nitrate in the Southern Ocean. Nitrate reductase activity is believed to control inorganic iodine speciation (IO₃⁻ or I⁻) in seawater; high concentrations of I⁻ (~100 nmol L⁻¹) are often present in surface subtropical water [Campos *et al.*, 1999]. The difference in the Chl-*a* normalized production rate of CH₃I between the warm oligotrophic subtropical water and euphotic tropical water might be associated with nitrate reductase activity and inorganic iodine speciation. Further research on the relationship between the CH₃I production rate and nitrate level will clarify the reason for the subtropical CH₃I maximum.

3.2.4. Relationship Between CH₃I Concentration, SST, and Saturation Anomaly

A scatterplot of CH₃I versus SST is shown in Figure 3b. Almost all the CH₃I concentrations in cold water with SSTs below 10°C were less than the overall average of 3.3 pmol L⁻¹. The baseline concentrations of CH₃I were approximately 0.57–1 pmol L⁻¹ in cold water (SST < 5°C) and 1–2 pmol L⁻¹ in warmer water

Table 6. Production Rates of CH₃I

Water Types	MLD (m)/Chl- <i>a</i> Ocean ^a /Month (n ^b)	MLD (m)/Chl- <i>a</i> ($\mu\text{g L}^{-1}$)	Temp. (°C)	Wind Speed (m s ⁻¹)	Conc. (pmol L ⁻¹)	Air-Sea Flux (nmol m ⁻² d ⁻¹)	Cl Loss (nmol m ⁻² d ⁻¹)	Net Production (pmol L ⁻¹ d ⁻¹)	Chl- <i>a</i> Normalized Production Rate ($\mu\text{mol g}^{-1} \text{d}^{-1}$)
<i>Polar</i>									
Arc/Sep–Oct (26)	16/0.72	2.1	8.4	1.2	3.0	0.03	0.2	0.5	
S/Dec–Jan (1)	10/0.53	-0.3	8.0	2.5	7.7	0.03	0.8	1.5	
<i>Subpolar</i>									
NW/Aug (8)	14/0.66	13.9	6.8	4.2	11.9	0.8	0.9	1.4	
<i>Transitional</i>									
NW/Jan (9)	92/0.53	3.5	6.5	1.6	2.5	0.3	0.03	0.06	
NW/May (4)	34/4.57	10.9	4.8	3.2	3.9	0.9	0.2	0.07	
NW/Aug (6)	19/0.19	23.5	5.1	4.0	8.5	4.3	0.7	4.0	
SI/Dec (1)	26/0.36	17.4	11.3	5.8	43.8	3.2	1.8	5.0	
<i>Subtropical</i>									
NW/Jun (4)	21/0.08	24.5	6.3	5.0	15.0	6.7	1.1	15.4	
NW/Sep (4)	35/0.05	28.9	4.6	5.6	11.7	26.5	1.1	26.3	
SI/Dec (2)	18/0.05	23.4	6.9	3.5	15.5	3.1	1.7	40.4	
<i>Tropical</i>									
I/Nov–Dec (6)	32/0.18	28.3	4.1	3.3	5.7	10.7	0.5	3.7	

^aArc: Arctic Ocean, S: Southern Ocean, NW: NW Pacific Ocean, SI: South Indian Ocean, I: North and South Indian Oceans.^bn: number of samples collected at CTD observation stations.

(SST > 5°C). The baseline level in polar water was slightly above supersaturation with respect to the atmospheric concentration. We calculated the saturation anomaly of CH₃I using equation (11).

$$\text{Saturation anomaly (SA)} = (p\text{CH}_3\text{I}_{\text{water}} - p\text{CH}_3\text{I}_{\text{air}}) / p\text{CH}_3\text{I}_{\text{air}}. \quad (11)$$

The average values of $p\text{CH}_3\text{I}_{\text{air}}$ and SA in each water type and area are summarized in Table 7. The basin averages of $p\text{CH}_3\text{I}_{\text{air}}$ in tropical-to-subpolar waters (0.68–1.1 patm) were within the range of the annual average values (0.5–1.1 patm) measured in marine air over tropical-to-subpolar oceans [Yokouchi *et al.*, 2008]. The polar basin average (0.50 patm) was similar to the mean value of 0.52 patm observed in September and October over the Arctic Ocean [Yokouchi *et al.*, 2013].

A positive SA value implies supersaturation of CH₃I in seawater. The lowest SA values (0.35–0.50) were measured in the polar waters of shelf and basin areas. Generally, subtropical basin water had the highest SA (61)

among all the water types and areas. The average for all basins (35) was higher than the slope (9.0) and shelf (6.5) average values. These results suggest that basin areas, particularly in subtropical water, have the highest potential to emit CH₃I to the air.

Table 7. Partial Pressure of CH₃I in the Marine Boundary Layer Air and Saturation Anomaly^a

Water Type	Air Partial Pressure (patm)	Saturation Anomaly
<i>Polar water</i>		
Basin	0.50 (0.32, 0.76)	6.2 (0.50, 15)
Slope	0.80 (0.60, 2.3)	1.5 (0.35, 3.6)
Shelf	0.97 (0.60, 2.3)	2.6 (0.36, 4.9)
<i>Subpolar water</i>		
Basin	1.1 (0.22, 2.3)	13 (2.9, 42)
Slope	1.0	5.5
Shelf	1.2 (1.0, 1.3)	3.9 (2.0, 7.1)
<i>Transition water</i>		
Basin	0.88 (0.32, 1.8)	33 (5.9, 92)
Slope	1.5 (0.72, 2.4)	9.9 (1.1, 31)
Shelf	1.3 (0.73, 2.6)	17 (2.0, 46)
<i>Subtropical water</i>		
Basin	0.68 (0.32, 1.2)	61 (18, 159)
Slope	0.68 (0.61, 0.73)	20 (14, 30)
Shelf	0.62 (0.61, 0.62)	20 (17, 23)
<i>Tropical water</i>		
Basin	0.82 (0.41, 2.1)	41 (11, 83)
<i>Total</i>		
Basin	0.85 (0.22, 2.3)	35 (0.44, 159)
Slope	1.1 (0.60, 2.4)	9.0 (0.35, 31)
Shelf	1.1 (0.50, 2.6)	6.6 (0.36, 46)

^aSaturation anomaly = ($p\text{CH}_3\text{I}_{\text{water}} - p\text{CH}_3\text{I}_{\text{air}}) / p\text{CH}_3\text{I}_{\text{air}}$.

3.2.5. Ethyl Iodide (C₂H₅I)

The average concentrations (min–max) of C₂H₅I in all water types in basin, slope, and shelf areas were 0.15 (DL–3.2), 0.23–0.24 (DL–2.5), and 0.59 (0.05–4.0) pmol L⁻¹, respectively. From the global map of C₂H₅I distribution, high concentrations of C₂H₅I (1.0–3.2 pmol L⁻¹) were present in the shelf-slope areas of the transitional western NW Pacific, where a phytoplankton boom occurred in May (Figure 6b; light blue-to-red symbols), and the shelf area of the Bering Sea in October (Figure 6c; green-to-red symbols). The high concentrations in highly productive areas are consistent with the average concentration (1.5 pmol L⁻¹) reported in bloom areas of the Baltic Sea [Karls-son *et al.*, 2008] and the average values for the Southern Ocean (0.1–2.8 pmol L⁻¹) [Abrahamsson *et al.*, 2004]. Low concentrations of C₂H₅I (<0.05 pmol L⁻¹)

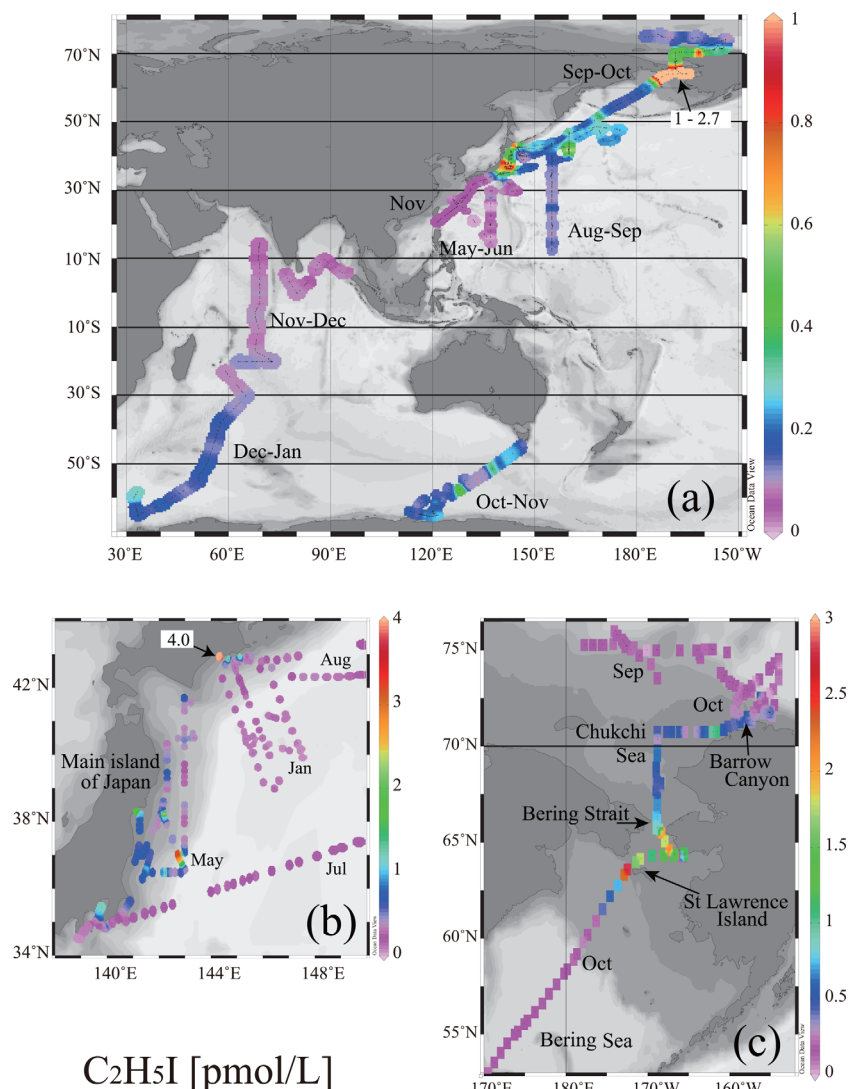


Figure 6. (a) Global-scale map of the horizontal distribution of $\text{C}_2\text{H}_5\text{I}$ concentrations in surface mixed layer water and (b) enlarged maps of $\text{C}_2\text{H}_5\text{I}$ concentrations in the western NW Pacific around Japan and (c) in the Bering Sea and Arctic Ocean. Numbers denoted in the figure with arrows show the concentrations over the color bar range, which were painted in cream-white color symbol.

were observed in basin areas of the subtropical NW Pacific and Indian Oceans (Figure 6a; purple symbols).

The concentration gradient of $\text{C}_2\text{H}_5\text{I}$, from high in shelf-slope areas to low in basin areas, is opposite to the CH_3I gradient, which is high in basin areas. Although the high-concentration areas of $\text{C}_2\text{H}_5\text{I}$ observed in highly productive transitional waters were largely consistent with the high-concentration areas of CH_3I , the average $\text{C}_2\text{H}_5\text{I}$ concentrations were lowest in oligotrophic subtropical waters characterized by low biological productivity, where the average CH_3I concentration was highest. Good correlations between $\text{C}_2\text{H}_5\text{I}$ and CH_3I concentrations ($R = 0.60\text{--}0.75$) occurred in shelf-slope areas of transitional, subpolar, and polar waters (Table 3). The good correlation of both these compounds in the coastal waters of the English Channel and in the North Sea have been attributed to similarities in production and loss processes in these areas, and the minimum concentration of $\text{C}_2\text{H}_5\text{I}$ in midsummer surface mixed layer water has been explained by photochemical removal processes [Archer *et al.*, 2007].

Our horizontal distribution results also suggest that the similarities in high-concentration areas of $\text{C}_2\text{H}_5\text{I}$ and CH_3I within high-productivity shelf-slope areas are the result of similarities in the biological production processes of both compounds. The observation that $\text{C}_2\text{H}_5\text{I}$ concentrations are low in subtropical waters, whereas those of CH_3I are high, can be explained by the higher rate of photolysis of $\text{C}_2\text{H}_5\text{I}$ than of CH_3I at high light

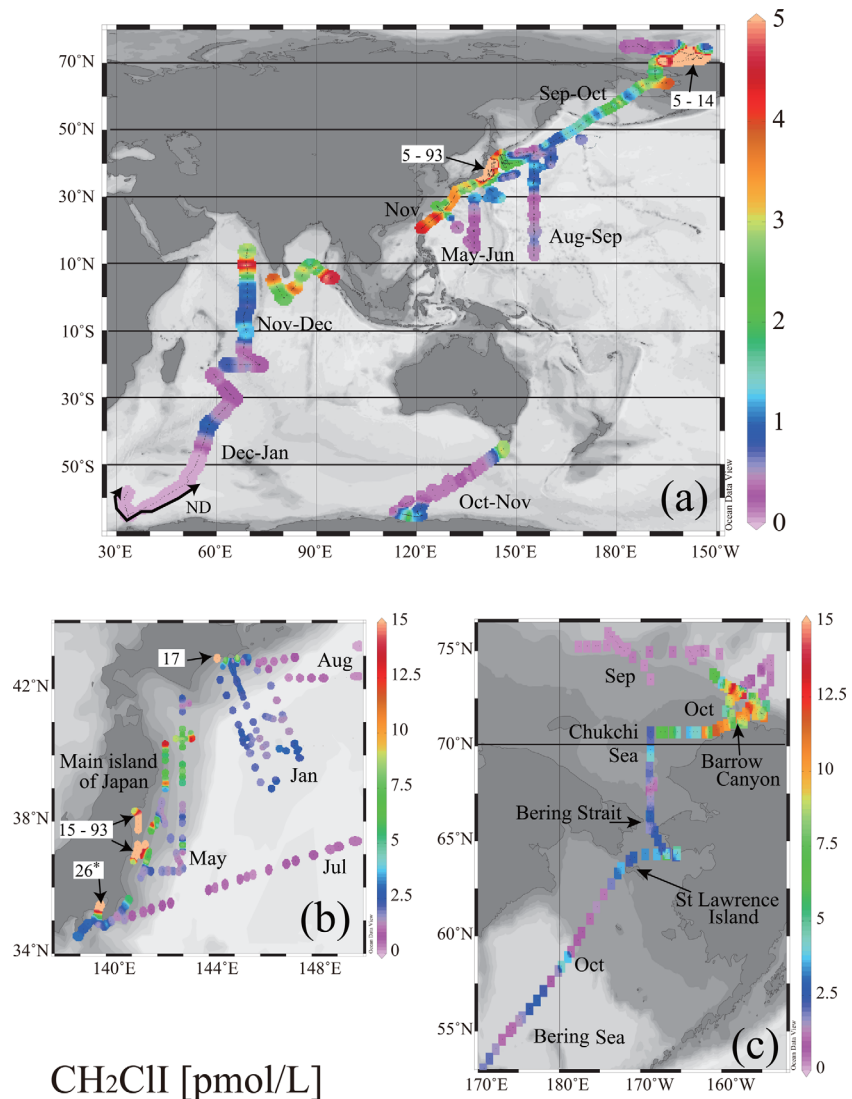


Figure 7. (a) Global-scale map of the horizontal distribution of CH_2ClI concentrations in surface mixed layer water and (b) enlarged maps of CH_2ClI concentrations in the western NW Pacific around Japan and (c) in the Bering Sea and Arctic Ocean. Numbers denoted in the figure with arrows show the concentrations over the color bar range, which were painted in cream-white color symbol.

intensities, particularly in the subtropical ocean. Similar trends have been demonstrated by long-term atmospheric monitoring of CH_3I and $\text{C}_2\text{H}_5\text{I}$ at subtropical Hateruma Island and subpolar Cape Ochiishi near the coasts of the NW Pacific [Yokouchi *et al.*, 2011].

3.2.6. Chloroiodomethane (CH_2ClI)

The average concentrations (min-max) of CH_2ClI in all water types in basin, slope, and shelf areas were 0.93–1.0 (DL-15), 3.7–3.8 (DL-19), and 6.6 (DL-93) pmol L^{-1} , respectively. From the global map of CH_2ClI distribution, the highest concentrations of CH_2ClI (15–93 pmol L^{-1} ; white plots in Figure 7b) were observed in shelf-slope areas of the transitional NW Pacific in May. The second highest concentrations (3–15 pmol L^{-1} ; yellow-red plots in Figure 7a and blue-red plots in Figures 7b and 7c) were observed on the shelf of the Chukchi Sea around Barrow Canyon, where there is a so-called biological hot spot in the Arctic Ocean because of the high rate of nutrient supply from regional upwelling [Mathis *et al.*, 2009], as well as the slope area vicinity of the highest area. Moderate concentrations (1–3 pmol L^{-1} ; blue-yellow plots in Figure 7a) were observed in basin areas of tropical, transitional, and subarctic waters. Low concentrations (<1 pmol L^{-1}) were present in the basin areas of the NW Pacific, Indian, and Southern Oceans (Figure 7a; purple symbols).

Table 8. Sea-Air Flux (nmol/m²/h) of VOIs, and Their Contributions (%) to the Total 3 VOI Flux in Parentheses^a

Water Type and Area	CH ₃ I	C ₂ H ₅ I	CH ₂ CII	Total VOI
<i>Polar water</i>				
Basin	0.24 (58%)	0.005–0.025 (4%)	0.14–0.18 (38%)	0.41
Slope	0.071 (9%)	0.003–0.016 (1%)	0.68–0.73 (90%)	0.79
Shelf	0.16 (17%)	0.056–0.070 (6%)	0.71–0.79 (77%)	0.97
<i>Subpolar water</i>				
Basin	0.53 (66%)	0.016–0.028 (3%)	0.21–0.29 (31%)	0.80
Slope	0.60 (72%)	0.023–0.046 (4%)	0.14–0.27 (24%)	0.84
Shelf	0.52 (33%)	0.31–0.33 (20%)	0.67–0.82 (47%)	1.6
<i>Transition water</i>				
Basin	0.68 (82%)	0.020–0.025 (3%)	0.11–0.14 (15%)	0.83
Slope	0.21 (52%)	0.022–0.023 (5%)	0.17–0.18 (43%)	0.41
Shelf	0.50 (29%)	0.046–0.048 (3%)	1.2 (68%)	1.7
<i>Subtropical water</i>				
Basin	0.71 (91%)	0.01–0.014 (2%)	0.045–0.069 (7%)	0.79
Slope	0.23 (35%)	0.003–0.005 (1%)	0.43 (65%)	0.67
Shelf	0.19 (33%)	0.003–0.004 (1%)	0.38–0.40 (67%)	0.58
<i>Tropical water</i>				
Basin	0.34 (54%)	0.006–0.008 (1%)	0.27–0.29 (44%)	0.63
<i>Total water type</i>				
Basin	0.58 (79%)	0.014–0.021 (2%)	0.12–0.15 (18%)	0.74
Slope	0.17 (31%)	0.012–0.016 (3%)	0.35–0.36 (67%)	0.54
Shelf	0.31 (25%)	0.098–0.11 (8%)	0.81–0.89 (67%)	1.3

^aThe average flux was calculated using the fixed range of $p\text{VOCl}_{\text{air}}$ (0–0.2 patm) when the data were below the detection limit (0.2 patm). The range of averaged flux is attributable to the fixed concentration range of the DL sample.

The concentration gradient of CH₂CII, from high in shelf-slope areas to low in basin areas, is similar to that of C₂H₅I. Photochemical removal of CH₂CII from the surface mixed layer water would be significant in basin areas, for C₂H₅I as well; however, correlations between CH₂CII and C₂H₅I concentrations in all water types and areas were not obtained. Poor correlation between these two compounds can be attributed to differences in photolysis rates and biological production processes. The photolysis rate of CH₂CII is several tens of times higher than that of C₂H₅I from atmospheric lifetime estimation [WMO, 2010]. The biological production processes of both compounds might be quite different from each other.

We noticed that higher concentrations of CH₂CII were present in basin areas of the western NW Pacific during January (1–2.5 pmol L⁻¹; blue symbols in Figure 7b) than for the same area during July and August (<1 pmol L⁻¹; purple symbols in Figure 7b). Based on the vertical profile of VOIs in seawater, the maximum concentrations of CH₂CII have often been observed in the subsurface layer, the depth of which is sometimes close to the subsurface chlorophyll maximum depth [Yamamoto et al., 2001]; surface minima are often present in stratified surface layer waters during summer. The concentration maximum in the subsurface layer has been attributed to biological production of CH₂CII, and the minima in the surface layer have been attributed to photolysis. The high concentrations of CH₂CII observed in the surface mixed layer waters of the western NW Pacific during the winter are probably due to two reasons: the first is due to the deep mixing of CH₂CII with subsurface waters, which could have accumulated the biologically produced CH₂CII during the summer; the second may be due to the slower photolysis rate in winter because of weak sunlight and the deep mixing. The high concentrations near the Asian continent's coast in November (Figure 7b; red symbols) may be caused by winter vertical mixing, and the high concentrations around the Barrow Canyon in the Arctic can be explained by regional upwelling. We can conclude that the concentrations of CH₂CII in surface mixed layer water are largely controlled by biological production of CH₂CII in the surface mixed layer as well as in the subsurface layer and the subsequent upwelling from the subsurface to surface mixed layer, and through losses to the air and photolysis. Therefore, high concentrations are often observed in the high-productivity shelf-slope areas, where biological production is high and the water mixing structure is more complex than the basin areas.

3.2.7. Sea-Air VOI Fluxes

The average fluxes of the VOIs are summarized in Table 8. The sum of the average fluxes of the three VOIs in basin, slope, and shelf areas for all water types were 0.74, 0.54, and 1.3 nmol m⁻² h⁻¹, respectively. In the basin areas, the total fluxes of all the VOIs were smallest in polar waters (0.41 nmol m⁻² h⁻¹). Total VOIs

fluxes in basin areas were higher in other waters (tropical, subtropical, transitional, and subpolar) and fell within a narrow range of 0.63–0.83 nmol m⁻² h⁻¹. The average fluxes of CH₃I, C₂H₅I, and CH₂CII in the basin areas were 0.58, 0.017, and 0.14 nmol m⁻² h⁻¹, respectively; these fluxes correspond to 79%, 2%, and 18% of the sum of the three VOI fluxes. The fluxes of CH₃I, C₂H₅I, and CH₂CII contributed 31%, 3%, and 67% of the total VOI fluxes in slope areas, respectively, and 25%, 8%, and 67% in shelf areas, respectively. We observed that the flux of CH₂CII was the highest among the three VOI fluxes in slope and shelf areas, whereas the flux of CH₃I was the highest in basin areas.

The average CH₃I flux of 0.58 nmol m⁻² h⁻¹ in the basin areas was consistent with the averages of 0.48–0.50 nmol m⁻² h⁻¹ in the open ocean of the North Atlantic (15°N–58°N) [Jones *et al.*, 2010] and 0.67 nmol m⁻² h⁻¹ in the North and South Pacific (40°N–40°S) [Moore and Groszko, 1999]. Jones *et al.* [2010] showed that the mean fluxes of CH₃I, C₂H₅I, and CH₂CII in the open ocean accounted for 53–55%, 2–3%, and 11–26% of the total iodine flux of six VOIs (CH₃I, C₂H₅I, CH₂CII, CH₂I₂, CH₂BrI, and C₃H₇I). They also indicated that the total iodine flux of dihalomethanes (CH₂CII, CH₂I₂, and CH₂BrI) was equal to that of CH₃I in the open ocean, and the total dihalomethane fluxes in shelf and coastal areas were 2 and 4 times higher than their respective CH₃I fluxes. Annual observations in the English Channel and the North Sea indicated that the mean fluxes of CH₃I, C₂H₅I, and CH₂CII were 0.5, 0.1, and 0.78 nmol m⁻² h⁻¹, respectively. These fluxes accounted for 36%, 7%, and 57% of the total VOI flux; CH₂CII was therefore, also the dominant contributor to the VOI flux in these shelf areas [Archer *et al.*, 2007]. Our results provide more detailed information about VOI fluxes from polar to tropical waters in shelf-slope-basin areas.

4. Conclusions

Shipboard observations were carried out on the continental shelf, slope, and basin areas of the Arctic, NW Pacific, Indian, and Southern Oceans to determine the horizontal distributions of the concentrations of C₅H₈, CH₃I, C₂H₅I, and CH₂CII in surface mixed layer water. The following list is a summary of the characteristics of the horizontal distributions of these chemicals and some hypotheses concerning the mechanisms responsible for their production and loss.

1. The highest concentrations of C₅H₈ were observed in highly productive areas. A scatterplot of C₅H₈ versus SST in the basin areas indicates that the maximum concentration occurs for SSTs in the range of 10–20°C, which is the range of SST that corresponds to the temperatures associated with phytoplankton blooms in transitional and subpolar waters. In the eutrophic tropical Indian Ocean, C₅H₈ concentrations were high where the SST was high (about 28°C). These results indicate that high C₅H₈ concentrations are associated with high biological productivity and suggest that, in the warm water where the high emitter of C₅H₈, such as *Prochlorococcus*, prevails in the biological community, high production rates of C₅H₈ would be found at the temperature that maximizes the photosynthesis rate of the community. The inconsistency between the high rates of C₅H₈ production in the warm waters obtained from our observations and the low rates of previously reported production rates obtained from phytoplankton incubation experiments would be attributed to the existence of a strong C₅H₈ emitter in warm waters which has not yet been sampled for the incubation experiment to measure the C₅H₈ production rates. Multiple-regression analysis provided empirical formulae to predict C₅H₈ concentrations from Chl-a concentration and SST, with overall coefficient of determination R² = 0.67.
2. High concentrations of CH₃I were observed in highly productive transitional waters and the oligotrophic subtropical NW Pacific over a wide range of latitudes, while the lowest concentrations and saturation anomalies were observed in the Arctic Ocean. The average SA in basin areas was higher than the average shelf and slope concentrations, suggesting that the basin areas have the largest potential to emit CH₃I to the air. A high production rate of CH₃I with Chl-a concentration in oligotrophic subtropical water implies the temperature-dependency of CH₃I production that might be associated with nutrient levels. This association with nutrient levels indicates an effect of nitrate reductase activity, which has been believed to control iodine speciation in seawater in previous studies.
3. High correlations (R > 0.60) between C₂H₅I and CH₃I concentrations were found in slope-shelf areas of cool transitional-subpolar-polar waters. High concentrations of C₂H₅I were observed in highly productive shelf-slope areas of transitional waters, where high concentrations of CH₃I were also present. In contrast, in oligotrophic subtropical water characterized by low biological productivity, the C₂H₅I concentrations

were low and the CH_3I concentrations were high. These results can be explained by the hypotheses that low concentrations of $\text{C}_2\text{H}_5\text{I}$ in subtropical waters are the result of a higher rate of photolysis of $\text{C}_2\text{H}_5\text{I}$ than that of CH_3I when the light intensity is high in summer, and that there is similarity in the biological production process of both these compounds in cool waters.

4. High concentrations of CH_2ClI in highly productive shelf-slope areas of the transitional NW Pacific in May can be attributed to the production of CH_2ClI at the surface mixed layer. Conversely, the concentrations of CH_2ClI in transitional waters of the NW Pacific were higher in winter than in summer. The relatively high concentrations in winter may be due to deep mixing with subsurface waters that accumulated CH_2ClI during the summer. The highest concentration, around Barrow Canyon in the shelf of the Arctic Ocean, can be explained by regional upwelling. The upwelling of subsurface water that has accumulated CH_2ClI by biological production through the high-productivity period is an important factor in raising CH_2ClI concentrations at the surface mixed layer.
5. Flux calculations show that the sea-to-air flux of CH_3I in basin areas form the largest contribution to the total VOI flux for all water types. In shelf-slope areas, the CH_2ClI flux has made the largest contribution to the total flux.

Acknowledgments

We thank the chief scientists, captains, and crews of the *Hokko-maru*, *Hakuho-maru*, *Tansei-maru*, *Mirai*, and *Aurora Australis*. We also thank K. Kuma for the measurements made during the *Mirai* cruise, and A. Tsuda for the chlorophyll-*a* measurement during the *Hakuho* and *Tansei* cruises. The measurements made during the *Hokko-maru* cruise, the *Hakuho-maru* cruises, and the *Tansei-maru* cruise were supported by a Grant-in-Aid for Scientific Research in Priority Areas "Western Pacific Air-Sea Interaction Study (W-PASS)" under grant 18067012. The W-PASS is a contribution to the Surface Ocean Lower Atmosphere Study (SOLAS) Core Project of the International Geosphere-Biosphere Programme (IGBP). The measurements during the *Mirai* cruise were supported by JSPS KAKENHI Grant 24681001 and the Arctic Climate Change Research Project under the Green Network of Excellence (GRENE). GRENE was initiated by the Ministry of Education, Culture, Sports, Science and Technology (MEXT) Japan. The measurements during the *Aurora Australis* cruise of the SIPEX-2 project were supported by the Australian Antarctic Project (4073). Our mapping data (C_5H_8 , CH_3I , $\text{C}_2\text{H}_5\text{I}$, and CH_2ClI) can access via supporting information of this paper.

References

- Abrahamsson, K., A. Loren, A. Wulff, and S. A. Wangberg (2004), Air-sea exchange of halocarbons: The influence of diurnal and regional variations and distribution of pigments, *Deep Sea Res., Part II*, 51(22–24), 2789–2805, doi:10.1016/j.dsrr.2004.09.005.
- Anilkumar, N., M. K. Dash, A. J. Luis, V. R. Babu, Y. K. Somayajulu, M. Sudhakar, and P. C. Pandey (2005), Oceanic fronts along 45°E across Antarctic Circumpolar Current during austral summer 2004, *Curr. Res.*, 88(10), 1669–1673.
- Archer, S. D., L. E. Goldson, M. I. Liddicoat, D. G. Cummings, and P. D. Nightingale (2007), Marked seasonality in the concentrations and sea-to-air flux of volatile iodocarbon compounds in the western English Channel, *J. Geophys. Res.*, 112, C08009, doi:10.1029/2006JC003963.
- Arnold, S. R., et al. (2009), Evaluation of the global oceanic isoprene source and its impacts on marine organic carbon aerosol, *Atmos. Chem. Phys.*, 9, 1253–1262, doi:10.5194/acp-9-1253-2009.
- Baker, A. R., S. M. Turner, W. J. Broadgate, A. Thompson, G. B. McFiggans, O. Vesperini, P. D. Nightingale, P. S. Liss, and T. D. Jickells, (2000), Distribution and sea-air fluxes of biogenic trace gases in the eastern Atlantic Ocean, *Global Biogeochem. Cycles*, 14(3), 871–886, doi:10.1029/1999GB001219.
- Bonsang, B., V. Gros, I. Peeken, N. Yassaa, K. Bluhm, E. Zoellner, R. Sarda-Esteve, and J. Williams (2010), Isoprene emission from phytoplankton monocultures: The relationship with chlorophyll-*a*, cell volume and carbon content, *Environ. Chem.*, 7(6), 554–563, doi:10.1071/EN09156.
- Broadgate, W. J., P. S. Liss, and S. A. Penkett (1997), Seasonal emissions of isoprene and other reactive hydrocarbon gases from the ocean, *Geophys. Res. Lett.*, 44(21), 2675–2678, doi:10.1029/97GL02736.
- Broadgate, W. J., G. Malin, F. C. Kupper, A. Thompson, and P. S. Liss (2004), Isoprene and other non-methane hydrocarbons from seaweeds: A source of reactive hydrocarbons to the atmosphere, *Mar. Chem.*, 88, 61–73, doi:10.1016/j.marchem.2004.03.002.
- Campos, M. L. A. M., R. Sanders, and T. Jickells (1999), The dissolved iodate and iodide distribution in the South Atlantic from the Weddell Sea to Brazil, *Mar. Chem.*, 65, 167–175.
- Carpenter, L. J., W. T. Sturges, S. A. Penkett, P. S. Liss, B. Aliche, K. Hebestreit, and U. Platt (1999), Short-lived alkyl iodides and bromides at Mace Head, Ireland: Links to biogenic sources and halogen oxide production, *J. Geophys. Res.*, 104(D1), 1679–1689, doi:10.1029/98JD02746.
- Carpenter, L. J., G. Malin, P. S. Liss, and F. C. Kupper (2000), Novel biogenic iodine-containing trihalomethanes and other short-lived halocarbons in the coastal East Atlantic, *Global Biogeochem. Cycles*, 14(4), 1191–1204, doi:10.1029/2000GB001257.
- Carpenter, L. J., S. D. Archer, and R. Beale (2012), Ocean-atmosphere trace gas exchange, *Chem. Soc. Rev.*, 41, 6473–6506, doi:10.1039/C2CS35121H.
- Chuck, A. L., S. M. Turner, and P. S. Liss (2005), Oceanic distributions and air-sea fluxes of biogenic halocarbons in the open ocean, *J. Geophys. Res.*, 110, C10022, doi:10.1029/2004JC002741.
- DeBruyn, W. J., and E. S. Saltzman (1997), Diffusivity of methyl bromide in water, *Mar. Chem.*, 57, 55–59, doi:10.1016/S0304-4203(96)00092-8.
- Elliott, S., and F. S. Rowland (1993), Nucleophilic substitution rates and solubilities for methyl halides in seawater, *Geophys. Res. Lett.*, 20(11), 1043–1046, doi:10.1029/93GL01081.
- Fuse, H., H. Inoue, K. Murakami, O. Takimura, and Y. Yamaoka (2003), Production of free and organic iodine by *Roseovarius* spp., *FEMS Microbiol. Lett.*, 229, 189–194, doi:10.1016/S0378-1097(03)00839-5.
- Guenther, A., et al. (1995), A global-model of natural volatile organic-compound emissions, *J. Geophys. Res.*, 100(D5), 8873–8892, doi:10.1029/94JD02950.
- Happell, J. D., and D. W. R. Wallace (1996), Methyl iodide in the Greenland/Norwegian Seas and the tropical Atlantic Ocean: Evidence for photochemical production, *Geophys. Res. Lett.*, 23(16), 2105–2108, doi:10.1029/2006JC003963.
- Hayase, S., A. Yabushita, and M. Kawasaki (2012), Iodine emission in the presence of humic substances at the water's surface, *Phys. Chem. A*, 116, 5779–5783, doi:10.1021/jp2048234.
- Jones, C. E., and L. J. Carpenter (2007), Chemical destruction of CH_3I , $\text{C}_2\text{H}_5\text{I}$, $1\text{-C}_3\text{H}_7\text{I}$, and $2\text{-C}_3\text{H}_7\text{I}$ in saltwater, *Geophys. Res. Lett.*, 34, L13804, doi:10.1029/2007GL029775.
- Jones, C. E., K. E. Hornsby, R. Sommariva, R. M. Dunk, R. von Glasow, G. McFiggans, and L. J. Carpenter (2010), Quantifying the contribution of marine organic gases to atmospheric iodine, *Geophys. Res. Lett.*, 37, L18804, doi:10.1029/2010GL043990.
- Karlsson, A., N. Auer, D. Schulz-Bull, and K. Abrahamsson (2008), Cyanobacterial blooms in the Baltic—A source of halocarbons, *Mar. Chem.*, 110(3–4), 129–139, doi:10.1016/j.marchem.2008.04.010.
- Kumar, S. P., and T. G. Prasad (1999), Formation and spreading of Arabian Sea high-salinity water mass, *J. Geophys. Res.*, 104(C1), 1455–1464, doi:10.1029/1998JC900022.

- Kurihara, M. K., et al. (2010), Distributions of short-lived iodocarbons and biogenic trace gases in the open ocean and atmosphere in the western North Pacific, *Mar. Chem.*, 118(3–4), 156–170, doi:10.1016/j.marchem.2009.12.001.
- Manley, S. L. (1992), Laboratory production of bromoform, methylene bromide, and methyl-iodide by macroalgae and distribution in near-shore Southern California Waters, *Limnol. Oceanogr.*, 37(8), 1652–1659, doi:10.4319/lo.1992.37.8.1652.
- Manley, S. L., and M. N. Dastoor (1987), Methyl halide (CH_3X) production from the giant kelp, *Macrocystis*, and estimates of global CH_3X production by kelp, *Limnol. Oceanogr.*, 32(3), 709–715, doi:10.4319/lo.1987.32.3.0709.
- Manley, S. L., and J. L. de la Cuesta (1997), Methyl iodide production from marine phytoplankton cultures, *Limnol. Oceanogr.*, 42(1), 142–147, doi:10.1029/2006JC003963.
- Mathis, J. T., N. R. Bates, D. A. Hansell, and T. Babila (2009), Net community production in the northeastern Chukchi Sea, *Deep Sea Res., Part II*, 56(17), 1213–1222, doi:10.1016/j.dsr2.2008.10.017.
- Matsunaga, S., M. Mochida, T. Saito, and K. Kawamura (2002), In situ measurement of isoprene in the marine air and surface seawater from the western North Pacific, *Atmos. Environ.*, 36(39–40), 6051–6057, doi:10.1016/S1352-2310(02)00657-X.
- Milne, P. J., D. D. Riener, and R. G. Zika (1995), Measurement of vertical distribution of isoprene in surface seawater, its chemical fate, and its emission from several phytoplankton monocultures, *Mar. Chem.*, 48(3–4), 237–244, doi:10.1016/0304-4203(94)00059-M.
- Moore, R. M., and W. Groszko (1999), Methyl iodide distribution in the ocean and fluxes to the atmosphere, *J. Geophys. Res.*, 104(C5), 11,163–11,171, doi:10.1029/1998JC000073.
- Moore, R. M., and R. Tokarczyk (1992), Chloro-iodomethane in N. Atlantic waters: A potentially significant source of atmospheric iodine, *Geophys. Res. Lett.*, 19(17), 1779–1782, doi:10.1029/92GL01796.
- Moore, R. M., and O. C. Zafiriou (1994), Photochemical production of methyl iodide in seawater, *J. Geophys. Res.*, 99(D8), 16,415–16,420, doi:10.1029/92GL01796.
- Moore, R. M., C. E. Geen, and V. K. Tait (1995), Determination of Henry's law constants for a suite of naturally occurring halogenated methanes in seawater, *Chemosphere*, 30, 1183–1191, doi:10.1029/2006GB002732.
- Mössinger, J. C., D. E. Shallcross, and R. A. Cox (1998), UV-VIS absorption cross-sections and atmospheric lifetimes of CH_2Br_2 , CH_2I_2 and CH_2BrI , *J. Chem. Soc. Faraday Trans.*, 94(10), 1391–1396, doi:10.1039/a709160e.
- Ohe, S. (2002), *Estimations of Physical Chemical Property* [Bussei Suisan-hou], DataBook Publ., Tokyo.
- Ooki, A., and Y. Yokouchi (2008), Development of a silicone membrane tube equilibrator for measuring partial pressures of volatile organic compounds in natural water, *Environ. Sci. Technol.*, 42(15), 5706–5711, doi:10.1021/es800912j.
- Ooki, A., and Y. Yokouchi (2011a), Dichloromethane in the Indian Ocean: Evidence for in-situ production in seawater, *Mar. Chem.*, 124(1–4), 119–124, doi:10.1016/j.marchem.2011.01.001.
- Ooki, A., and Y. Yokouchi (2011b), Determination of Henry's law constant of halocarbons in seawater and analysis of sea-to-air flux of iodoethane ($\text{C}_2\text{H}_5\text{I}$) in the Indian and Southern Oceans based on partial pressure measurements, *Geochem. J.*, 45(6), E1–E7.
- Ooki, A., A. Tsuda, S. Kameyama, S. Takeda, S. Itoh, T. Suga, H. Tazoe, A. Okubo, and Y. Yokouchi (2010), Measurements of methyl halides in surface seawater and marine boundary layer of Northwest Pacific, *J. Geophys. Res.*, 115, C10013, doi:10.1029/2009JC005703.
- Palmer, P. I., and S. L. Shaw (2005), Quantifying global marine isoprene fluxes using MODIS chlorophyll observations, *Geophys. Res. Lett.*, 32, L09805, doi:10.1029/2005GL022592.
- Quack, B., and D. W. R. Wallace (2003), Air-sea flux of bromoform: Controls, rates, and implications, *Global Biogeochem. Cycles*, 17(1), 1023, doi:10.1029/2002GB001890.
- Richter, U. (2003), Factors influencing methyl iodide production in the ocean and its flux to the atmosphere, PhD thesis, 117 pp., Kiel Univ., Kiel, Germany.
- Richter, U., and D. W. R. Wallace (2004), Production of methyl iodide in the tropical Atlantic Ocean, *Geophys. Res. Lett.*, 31, L23S03, doi:10.1029/2004GL020779.
- Roehl, C. M., J. B. Burkholder, G. K. Moortgat, A. R. Ravishankara, and P. J. Crutzen (1997), Temperature dependence of UV absorption cross sections and atmospheric implications of several alkyl iodides, *J. Geophys. Res.*, 102(11D), 12,819–12,829, doi:10.1029/97JD00530.
- Saito, H., A. Tsuda, and H. Kasai (2002), Nutrient and plankton dynamics in the Oyashio region of the western subarctic Pacific Ocean, *Deep Sea Res., Part II*, 49, 5463–5486, doi:10.1016/S0967-0645(02)00204-7.
- Schall, C., and K. G. Heumann (1993), GC determination of volatile organoiodine and organobromine compounds in Arctic seawater and air samples, *Fresenius J. Anal. Chem.*, 346(6–9), 717–722, doi:10.1016/S0967-0645(02)00204-7.
- Sharkey, T. D., and S. S. Yeh (2001), Isoprene emission from plants, *Annu. Rev. Plant Physiol. Plant Mol. Biol.*, 52, 407–436, doi:10.1146/annurev.arplant.52.1.407.
- Sharqawy, M. H., J. H. Lienhard, and S. M. Zubair (2010), Thermophysical properties of seawater: A review of existing correlations and data, *Desalin. Water Treat.*, 16, 354–380, doi:10.5004/dwt.2010.1079.
- Shaw, S. L., S. W. Chisholm, and R. G. Prinn (2003), Isoprene production by *Prochlorococcus*, a marine cyanobacterium, and other phytoplankton, *Mar. Chem.*, 80, 227–245, doi:10.1016/S0304-4203(02)00101-9.
- Simó, R., and J. Dachs (2002), Global ocean emission of dimethylsulfide predicted from biogeophysical data, *Global Biogeochem. Cycles*, 16(4), 1078, doi:10.1029/2001GB001829.
- Smythe-Wright, D., S. M. Boswell, P. Breithaupt, R. D. Davidson, C. H. Dimmer, and L. B. E. Diaz (2006), Methyl iodide production in the ocean: Implications for climate change, *Global Biogeochem. Cycles*, 20, GB3003, doi:10.1029/2005GB002642.
- Tran, S., B. Bonsang, V. Gros, I. Peeken, R. Sarda-Esteve, A. Bernhardt, and S. Belviso (2013), A survey of carbon monoxide and non-methane hydrocarbons in the Arctic Ocean during summer 2010, *Biogeosciences*, 10, 1909–1935, doi:10.5194/bg-10-1909-2013.
- Varner, R. K., Y. Zhou, R. S. Russo, O. W. Wingenter, E. Atlas, C. Stroud, H. Mao, R. Talbot, and B. C. Sive (2008), Controls on atmospheric chloroiodomethane (CH_2ClI) in marine environments, *J. Geophys. Res.*, 113, D10303, doi:10.1029/2007JD008889.
- Wanninkhof, R. (1992), Relationship between wind-speed and gas-exchange over the ocean, *J. Geophys. Res.*, 97(C5), 7373–7382, doi:10.1029/92JC00188.
- Welshmeyer, N. A. (1994), Fluorometric analysis of chlorophyll *a* in the presence of chlorophyll *b* and pheophytins, *Limnol. Oceanogr.*, 39(8), 1985–1992, doi:10.4319/lo.1994.39.8.1985.
- Wilke, C. R., and P. Chang (1955), Correlation of diffusion coefficients in dilute solutions, *AIChE J.*, 1(2), 264–270, doi:10.1002/aic.69001022.
- World Meteorological Organization (WMO) (2010), Scientific assessment of ozone depletion: 2006, *Global Res. Monit. Proj. Rep.* 52, Geneva.
- Yamamoto, H., Y. Yokouchi, A. Otsuki, and H. Itoh (2001), Depth profiles of volatile halogenated hydrocarbons in seawater in the Bay of Bengal, *Chemosphere*, 45(3), 371–377, doi:10.1029/2006jc003963.
- Yasuda, I. (2003), Hydrographic structure and variability in the Kuroshio-Oyashio transition area, *J. Oceanogr.*, 59(4), 389–402, doi:10.1029/2004GL021410.

- Yokouchi, Y., Y. Nojiri, L. A. Barrie, D. Toom-Sauntry, and Y. Fujinuma (2001), Atmospheric methyl iodide: High correlation with surface sea-water temperature and its implications on the sea-to-air flux, *J. Geophys. Res.*, 106(D12), 12,661–12,668, doi:10.1029/2001JD900083.
- Yokouchi, Y., et al. (2008), Global distribution and seasonal concentration change of methyl iodide in the atmosphere, *J. Geophys. Res.*, 113, D18311, doi:10.1029/2008JD009861.
- Yokouchi, Y., T. Saito, A. Ooki, and H. Mukai (2011), Diurnal and seasonal variations of iodocarbons (CH_2ClI , CH_2I_2 , CH_3I , and $\text{C}_2\text{H}_5\text{I}$) in the marine atmosphere, *J. Geophys. Res.*, 116, D06301, doi:10.1029/2010JD015252.
- Yokouchi, Y., Y. Nojiri, D. Toom-Sauntry, P. Fraser, Y. Inuzuka, H. Tanimoto, H. Nara, R. Murakami, and H. Mukai (2012), Long-term variation of atmospheric methyl iodide and its link to global environmental change, *Geophys. Res. Lett.*, 39, L23805, doi:10.1029/2012GL053695.
- Yokouchi, Y., J. Inoue, and D. Toom-Sauntry (2013), Distribution of natural halocarbons in marine boundary air over the Arctic Ocean, *Geophys. Res. Lett.*, 40(15), 4086–4091, doi:10.1002/grl.50734.
- Zindler, C., C. A. Marandino, H. W. Bange, F. Schutte, and E. S. Saltzman (2014), Nutrient availability determines dimethyl sulfide and isoprene distribution in the eastern Atlantic Ocean, *Geophys. Res. Lett.*, 41, 3181–3188, doi:10.1002/2014GL059547.
- Ziska, F., et al. (2013), Global sea-to-air flux climatology for bromoform, dibromomethane and methyl iodide, *Atmos. Chem. Phys.*, 13(17), 8915–8934, doi:10.5194/acp-13-8915-2013.